International Journal of Pharmaceutics: X 5 (2023) 100174

Contents lists available at ScienceDirect

International Journal of Pharmaceutics: X

journal homepage: www.sciencedirect.com/journal/international-journal-of-pharmaceutics-x

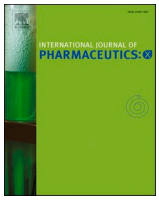

Development of thermosensitive hydrogel of Amphotericin-B and Lactoferrin combination-loaded PLGA-PEG-PEI nanoparticles for potential eradication of ocular fungal infections: *In-vitro*, *ex-vivo* and *in-vivo* studies

Sammar Fathy Elhabal [a], Shrouk A. Ghaffar [b], Raghda Hager [c], Nahla A. Elzohairy [d,e], Mohamed Mansour Khalifa [f,g], Passant M. Mohie [h], Rania A. Gad [i], Nasreen N. Omar [j], Mohammed H. Elkomy [k,*], Mohammad Ahmad Khasawneh [l,*], Nashwa Abdelaal [m]

[a] *Department of Pharmaceutics and Industrial Pharmacy, Faculty of Pharmacy, Modern University for Technology and Information (MTI), Mokattam, Cairo 11571, Egypt*
[b] *Tactical Medical Department, Caduceus Lane Healthcare, Alexandria 21532, Egypt*
[c] *Department of Medicinal Microbiology and Immunology, Faculty of Medicine King Salman International University, El-Tor, South Siniai, Egypt*
[d] *Air Force Specialized Hospital, Cairo 19448, Egypt*
[e] *Department of Microbiology and Immunology, Faculty of Pharmacy, Modern University for Technology and Information (MTI), Mokattam, Cairo 11571, Egypt*
[f] *Department of Human Physiology, Faculty of Medicine, Cairo University, Egypt*
[g] *Department of Human Physiology, College of Medicine, King Saud University, 62511, Saudi Arabia*
[h] *Department of Clinical Pharmacology, Faculty of Medicine, Alexandria University, Alexandria 21532, Egypt*
[i] *Department of Pharmacology and Toxicology, Faculty of Pharmacy, Nahda University, Beni-Suef (NUB), Beni-Suef, 62511, Egypt*
[j] *Department of Biochemistry, Faculty of Pharmacy, Modern University for Technology and Information (MTI), Mokattam, Cairo 11571, Egypt*
[k] *Department of Pharmaceutics, College of Pharmacy, Jouf University, Sakaka 72341, Saudi Arabia*
[l] *Department of Chemistry, College of Science U.A.E. University, Al-Ain, P.O. Box 17551, United Arab Emirates*
[m] *Department of Integrative Physiology, Baylor College of Medicine, Houston, TX, USA*

ARTICLE INFO

Keywords:
Amphotericin-B
Lactoferrin
Candida albicans
Confocal laser scanning microscopy (CLSM)
Draize test
Nanoparticles
Triblock polymers PLGA-PEG-PEI
Atomic force microscopy (AFM)

ABSTRACT

The most prevalent conditions among ocular surgery and COVID−19 patients are fungal eye infections, which may cause inflammation and dry eye, and may cause ocular morbidity. Amphotericin-B eye drops are commonly used in the treatment of ocular fungal infections. Lactoferrin is an iron-binding glycoprotein with broad-spectrum antimicrobial activity and is used for the treatment of dry eye, conjunctivitis, and ocular inflammation. However, poor aqueous stability and excessive nasolacrimal duct draining impede these agens' efficiency. The aim of this study was to examine the effect of Amphotericin-B, as an antifungal against *Candida albicans*, *Fusarium,* and *Aspergillus flavus*, and Lactoferrin, as an anti-inflammatory and anti-dry eye, when *co*-loaded in triblock polymers PLGA-PEG-PEI nanoparticles embedded in P188-P407 ophthalmic thermosensitive gel. The nanoparticles were prepared by a double emulsion solvent evaporation method. The optimized formula showed particle size (177.0 ± 0.3 nm), poly-dispersity index (0.011 ± 0.01), zeta-potential (31.9 ± 0.3 mV), and entrapment% (90.9 ± 0.5) with improved *ex-vivo* pharmacokinetic parameters and *ex-vivo* trans-corneal penetrability, compared with drug solution. Confocal laser scanning revealed valuable penetration of fluoro-labeled nanoparticles. Irritation tests (Draize Test), Atomic force microscopy, cell culture and animal tests including histopathological analysis revealed superiority of the nanoparticles in reducing signs of inflammation and eradication of fungal infection in

Abbreviations: PLGA, Poly (lactic-co-glycolic acid); PEG, polyethylene glycol; PEI, poly-ethylene imine; BLF, Bovine Lactoferrin; AMP, Amphotericin-B; J, steady-state flux; BCS, Biopharmaceutical Classification System; P407, Poloxamer 407; P188, Kolliphor®P188; EDC, ethyl-3-(3-dimethyl aminopropyl) carbodiimide; NHS, N-hydroxysuccinimide; REC, rules of the Study Ethics Committee; O, organic phase; A, aqueous phase; NPs, nanoparticles; FT-IR, Fourier transform infrared; DSC, Differential scanning calorimetry; TEM, Transmission electron microscopy; Kp, permeability coefficient; Q24, amount penetrated after 24 h; NCCLS, National Committee for Clinical Laboratory Standards; MIC, minimum inhibitory concentration; DMSO, dimethyl sulfoxide; HCE-2, human corneal epithelial cells; GRAS, Generally recognized as a safe; LPS, Lipopolysaccharide; CD14, Cluster of differentiation 14; ANOVA, Analysis of variance; CK, Creatine kinase; DLS, dynamic light scattering; EE%, Entrapment efficiency; QR, Quantity retained; FT-IR, Fourier-transform infrared spectroscopy; PBS, Phosphate buffered saline solution; PDI, Polydispersity index; PS, Particle size; SD, Standard deviations; SE, Standard error; SEM, Scanning electron microscope; ZP, Zeta potential..

* Corresponding authors.
E-mail addresses: Sammar.Fathy@pharm.mti.edu.eg (S.F. Elhabal), mhalkomy@ju.edu.sa (M.H. Elkomy), mohammad.khasawneh@uaeu.ac.ae (M.A. Khasawneh).

https://doi.org/10.1016/j.ijpx.2023.100174
Received 19 December 2022; Received in revised form 24 February 2023; Accepted 24 February 2023
Available online 28 February 2023

rabbits, without causing any damage to rabbit eyeballs. The nanoparticles exhibited favorable pharmacodynamic features with sustained release profile, and is neither cytotoxic nor irritating *in-vitro* or *in-vivo*. The developed formulation might provide a new and safe nanotechnology for treating eye problems, like inflammation and fungal infections.

1. Introduction

Ocular inflammation, including keratoconjunctivitis sicca, microbial infection-linked inflammation, post-operative inflammation, seasonal allergic conjunctivitis, blepharitis, or uveitis, can lead to potentially dangerous eye problems such as glaucoma or cataract if left untreated (Rehab et al., 2021). Viral ocular inflammation observed as a post-COVID-19 side effect in some patients is represented by conjunctivitis, fungal infection, cranial nerve palsies, and microvascular abnormalities in the retina (Mrittika et al., 2021).

Treatment of fungal and viral inflammation, and dry eye is difficult due to natural ocular barriers, such as the corneal epithelium and tear fluid, which limit medication access. There are no efficient drug delivery formulations available when ocular inflammation and tear film osmolality increase, leading to dry eye (Christopher et al., 2021& Lemp and Foulks, 2007). Additionally, developed drug resistance limits the use of the few available anti-fungal treatments such as azole, echinocandin, and polyene (Rajendra et al., 2016). Corticosteroids, antihistamines, and nonsteroidal anti-inflammatory drugs are also viable choices for the management of ocular inflammation. Nonetheless, long-term use of these medications, alone or in combination, is linked to considerable negative effects (Emily et al., 2020& Sanaa et al., 2018).

Amphotericin-B (AMP) is an antifungal polyene antibiotic isolated from Streptomyces. AMP tampers with cell membrane permeability, allowing leakage of intracellular components (H^+, Cl^-, Na^+, and K^+) followed by fungal cell death (Christopher et al., 2021& Lemp and Foulks, 2007). For >30 years, AMP has been available as the first commercially significant anti-fungal drug due to its ability to inhibit fungus growth by interacting with sterol molecules in fungal cell membranes, resulting in the formation of a complex ergosterol-AMP. This results in the development of holes and intracellular ion leakage, eventually resulting in fungal cell destruction and death (Falah and Obayes, 2020). AMP is used to treat AIDS-related fungal infections, candidiasis, para coccidioidomycosis, cryptococcosis, histoplasmosis, blastomycosis, extracutaneous sporotrichosis, aspergillosis, as well as certain hyalohyphomycotic and phaeohyphomycotic cases. The most common AMP formulation is AMP deoxycholate (Fungizone®), generally administered as an injection. Typical antifungal formulations, such as eye drops, have poor medication absorption and corneal bioavailability. Ophthalmic antifungal agents are not commercially available in many countries (Vogelsinger et al., 2006). The antifungal agent doesn't dissolve well in water and has a high molecular weight, which could make it hard for the drug to get into the cornea (Ahmed et al., 2021). Bovine Lactoferrin (BLF) is a naturally occurring three-dimensional glycoprotein generated by exocrine glands and neutrophils (Wang et al., 2019). BLF can be traced in tears, saliva, and gastrointestinal secretions, though it is most abundant in colostrum and milk (Valentina et al., 2019). BLF plays an important role in immunological regulation and defense mechanisms against bacteria and fungi, and immune expression in breast cancer and viruses, and exhibits remarkable safety features when delivered systemically at high dose concentrations (Alaaeldin et al., 2022 & Revu et al., 2021). Also, by acting on the resurgence of immunity in diabetic patients, an increase in serum BLF content may play a key role in restoring the immune balance to its optimal condition (Alaaeldin et al., 2022). BLF and hydrophilic substances leave the eye fast through the conjunctiva and the nasolacrimal duct (El-Desouky et al., 2017). BLF has the ability to reverse dry eye symptoms and possesses anti-inflammatory efficacy, without inducing ocular irritation. Hence, BLF has been suggested as a suitable approach in the treatment of dry eye disease (Ana et al., 2021).

Many features of the Biopharmaceutical Classification System (BCS) class IV drugs, such as AMP, make oral and peroral administration challenging. Low water solubility, irregular and poor absorption and poor permeability are some of these concerns. As a result, in situations when the medicine's therapeutic effect is directly required, a targeted drug delivery technique may be effective (*e.g.*, eye drops and topical eye gel preparations). This approach adds the advantage of the ease of administration of the drug in liquid form (Ghadi and Dand, 2017 & Sanaa et al., 2018). High concentration and frequent antifungal medicine administration for an extended period of time may result in side effects, poor compliance, and cost difficulties. Consequently, a drug carrier with greater penetration and retention characteristics is required. Active ocular administration *via* controlled release systems has arisen in recent years due to increased permeability, bioavailability, and stability, resulting in considerable benefits over standard pharmaceutical dose forms. Medication has been encapsulated into biodegradable polymeric nanoparticles (NPs) to address concerns of ocular tissue stability, therapeutic efficacy, and half-life, allowing for prolonged release (Rehab et al., 2021).

Poly (lactic-*co*-glycolic acid) (PLGA), a biodegradable and biocompatible aliphatic polyester, has long been an attractive material for drug delivery applications since it is FDA-approved for humans. Surface modification of PLGA NPs with polyethylene glycol (PEG) can further increase the long circulation characteristics of the NPs. The positive charge on the surface of polyethylene imine (PEI) may assist NPs to enter the cornea. PLGA matrices are commonly used to encapsulate hydrophobic and hydrophilic medicines. In a nutshell, the medication is dissolved in the organic phase with the polymer before being emulsified in the aqueous phase (Rebecca and Rachael, 2013).

BLF was found to be significantly synergistic with AMP in fungal species when formulated in tri-block polymer modification, because of the higher permeability, stability, and utilization rate of the loaded drug. This method of medication can reach the ocular space *via* transcellular, paracellular, or a combination of both routes. Chemical and structural improvements of BLF to function as an efficient anti-fungal adjuvant, are highly feasible in the future (Kenya et al., 2020).

The main objective of this work is the development of a new ophthalmic drug-delivery system for the treatment of both ocular inflammations and fungal eye infections. Although new medication delivery technologies such as Eudragit RL 100 based nanoparticles, liposomes and colloidal dispersions were found effective in facilitating ocular delivery of AMP, these systems were unstable (Swarnali et al., 2010). Consequently, the current study sought to investigate the improved topical efficacy, safety, penetrability, sustained drug delivery, adhesion, and therapeutic effect of triblock polymer NPs loaded with AMP, BLF, and the combination of both agents, after embedding in thermosensitive gel formulations, for treating fungal eye infection, dry eye, and inflammation conjunctivitis in a series of carefully designed *in-vitro* and *in-vivo* experiments using human corneal epithelial cells and rabbits, respectively. As far as we know, this is the first attempt to formulate the combination of AMP and BLF in a nano-based delivery system.

2. Materials and methods

2.1. Drugs, chemicals, and reagent kits

AMP was purchased from Cayman Chemical (Michigan, USA),

Azienda Chemical Pharmaceutica (Italy) supplied BLF, dimethyl sulfoxide (DMSO), formaldehyde, Ketoconazole; Boehringer Ingelheim (Germany) supplied PLGA, Kolliphor®P188(P188), ethyl acetate, Poloxamer P407, PEG, PEI, ethyl-3-(3-dimethyl aminopropyl) carbodiimide (EDC), Sodium arachidonate (SA, 0.5%), N-hydroxy succinimide (NHS). Keratinocyte serum-free medium, bovine pituitary extract, insulin, fetal bovine serum, IL-8, and TNF-α Human ELISA Kit, streptomycin, and penicillin were all donated by ThermoFisher Scientific (Life Technologies, CA, USA). A human corneal epithelial cell line immortalized by a hybrid adenovirus 12-SV40 virus (HCE-2, ATCC® CRL-11135) was donated by LGC Standards (Barcelona, Spain). For all tests, water filtration was achieved by employing the Millipore® MilliQ system. All additional solvents and chemicals were of analytical quality and were used as provided.

2.2. Animals

Forty-eight New Zealand albino male rabbits aged between 10 and 12 weeks and weighing between 2 and 2.5 kg were housed at 25 °C and 55–65% relative humidity through out the experimentation period. The animals were included in this study once obtained from Cairo University's Faculty of Pharmacy's Animal House in Giza, Egypt. All research procedures were authorized by the National Research Center's Animal Care Ethics Committee (PI 2334 on 31/12/2018) and animal tests followed the rules of the Study Ethics Committee (REC) established by Cairo University's Faculty of Pharmacy. In this work, rabbits were used and cared for in accordance with the ARVO statement on animal usage in ophthalmology and vision research, in addition to the European Union Directive on Animal Experimentation.

All rabbits were initially examined using a slit lamp and fluorescein to determine that the anterior eye segment was clinically healthy. Rabbits were randomly assigned to two groups Group one was employed to test the *in-vivo* antifungal activity of thermosensitive gel containing AMP-NPs, BLF-NPs or AMP-BLF-NPs, AMP-BLF solution, and Ketoconazole (each subgroup consisted of 6 rabbits) and Group two to test *ex-vivo* AMP and BLF corneal permeation from thermosensitive gel containing AMP-NPs, BLF-NPs or their combination.

2.3. Fungal strains

All standard fungal strains of *Candida albicans* (RCMB 005003), *Fusarium* (RCMB 080352), and *Aspergillus flavus* (RCMB 00200) were obtained from the Regional Center for Mycology and Biotechnology (RCMB) at Al-Azhar University in Cairo, Egypt. Sample collection and fungal isolation were according to the direct inoculation technique. On potato dextrose agar, the isolates were grown at 35 °C for 4–14 days, and the grown strains were preserved at 20 °C, in a stock solution of glycerol, for further use.

2.4. Preparation of studied strain

The inoculum size for all fungal isolates was adjusted using the McFarland scale. At 530 nm, a spectrophotometer (CM-600D Konica-Minolta, Osaka, Japan) was utilized to adjust the turbidity to 0.5 McFarland. Densities were $1.5^{-5}\times 10^{6}$ CFU/mL for *Candida albicans*, 0.4×10^{4} CFU/mL for *Fusarium*, and $2^{-3}\times 10^{4}$ CFU/mL for *Aspergillus*. In all investigations, these concentrations served as the standard inoculum. This suspension was used for ocular animal inoculation.

2.5. Method

2.5.1. Experimental design

The thermosensitive gel containing drug-loaded NPs was formulated by Multilevel categoric design comprising nine formulae for each drug, and then the best formula for each drug was chosen to make the combination. The studied factors were: Drugs: PLGA (Ratio) (A) and P407: P188 (Ratio) (B), all at three levels defined as (−1, 0, +1). Percent entrapment efficiency (EE %) (Y1), particle size (PS) (Y2), polydispersity index (PDI) (Y3), zeta potential (ZP) (Y4), and *in-vitro* release after 48 h (Q48h) (Y5) were studied using Design expert® version 10 (Stat Ease, Inc., Minneapolis, MN, USA), as the response variables, in order to determine the relevance of the investigated factors (David et al., 2019). The presentation of the central composite design with the levels of the independent variables and the constraints imposed on the accompanying response variables are shown in Table 1.

2.5.2. Preparation of triblock PLGA-PEI-PEG NPs-loaded P188-P407/PVA gel

A solution of 100 mg PLGA (dissolved in 50 mL dichloromethane) and a mixture of 100 mg PEI, 50 mg PEG, 5 mg EDC, and 5 mg NHS (dissolved in 50 mL methanol), were mixed and refluxed for eight hours at 50 °C for induction of the reaction. After the reaction was complete, the solvent was removed by rotary evaporation at 150 rpm, 40 °C, and 30 mL of deionized water was added to allow ultrasound dissolution (A1) (Lamprecht et al., 2000). In a dialysis bag, the aqueous solution was dialyzed with deionized water overnight (interception molecular weight = 10,000 Da) (S'anchez-L'opez et al., 2016). In addition, EDC, NHS, and 100 mg of (A1) were added to a beaker, and the solution was combined and agitated for eight hours in order to produce PLGA-PEI-PEG. In a beaker containing 10 mL of (A1) solution, 50 mg of tween 80 and AMP were added and agitated for 30 min. BLF was then introduced and ultrasonically mixed for 30 min, followed by 8 hours of stirring. The solution was then centrifuged (10,000 rpm/min) for 30 min to collect NPs (A2) for later use (Gonzalez-Pizarro et al., 2019a, 2019b). The thermosensitive gel was prepared by dissolving 25 g of poloxamer P407 and 3 g poloxamer P188 in 70 mL of deionized water and storing at 4 °C. 500 mg of the best formulation NPs was added to the temperature-sensitive gel, which was then mixed and chilled at 4 °C (Gonzalez-Pizarro et al., 2019a) as shown in (Fig. 1).

2.6. In vitro characterization of the prepared AMP and BLF loaded Tri block polymers PLGA-PEG-PEI NPs

2.6.1. Determination of entrapment efficiency (EE%)

Percent of entrapment efficiency (EE %) of NPs was estimated by the determination of free AMP and BLF (unentrapped AMP and BLF) in an indirect way (Desiree et al., 2019). Using a cooling centrifuge (Beckman Optima®, Ultracentrifuge, California, USA) operated at 21,000 rpm, the resulting formula (1 mL) was processed for 60 min at 4 °C. Following isolation of the clear supernatant, the concentrations of unentrapped AMP and BLF were determined using HPLC (C18 column 250 × 4.6 mm, 5 μm particle size) (Shimadzu, Kyoto, Japan), preceded by a guard column (45 × 4.6 mm). At room temperature, the mobile phase was prepared to consist of acetonitrile: acetic acid (1%): water (4:43:16 *v*/v)

Table 1
Independent variables levels as designated by the categorical multilevel factorial design, along with the measured dependent responses and their desirability constraints.

Factor (Independent variable)	Level		
	-1	0	+1
A: Drugs: PLGA Ratio	1:2	1:5	1:10
B: P407:P188 Ratio	1:5	1:10	1:15

Response (Dependent Variable)	Desirability Constraints
Y1:EE%	Maximize
Y2:PS (nm)	Minimize
Y3: PDI	Minimize
Y4: ZP (absolute value) (mV)	Maximize
Y5:Q48h (%)	>80%

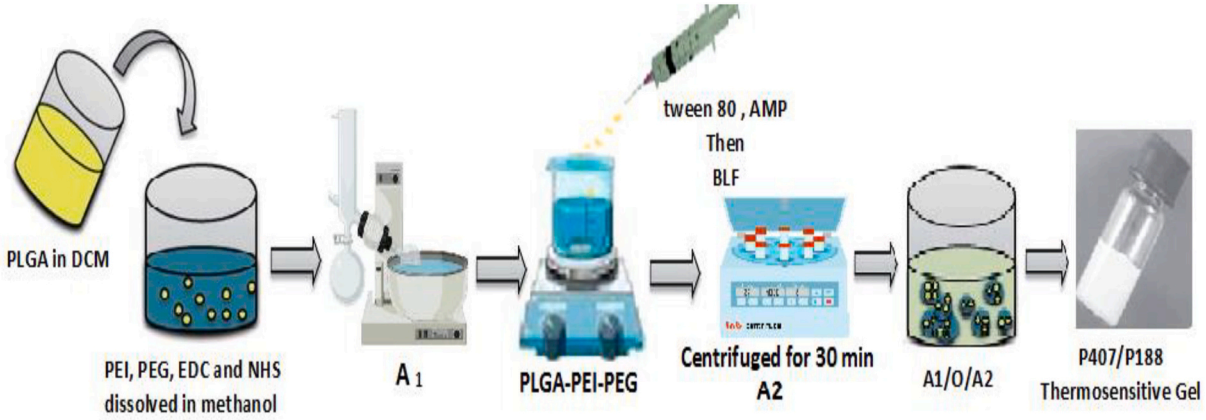

Fig. 1. Graphic representation of the method employed for the preparation of AMP and BLF triblock polymer PLGA-PEG-PEI NPs by using double emulsion solvent evaporation method. PLGA: Poly (lactic-*co*-glycolic acid); PEG: polyethylene glycol; PEI: poly-ethylene imine; BLF: Bovine Lactoferrin; AMP: Amphotericin-B; P407: Poloxamer-407; P188: Kolliphor®P188; EDC: ethyl-3-(3-dimethyl aminopropyl) carbodiimide NHS: N-hydroxysuccinimide.

and was injected at a rate of flow of 1.5 mL/min and the injection volume was 20 µL. An SPD-M10Avp diode array UV detector was used to detect at 405 nm (Shimadzu, Kyoto, Japan). Retention times were calculated to be 4.3 and 11.1 min for AMP and BLF, respectively. By using calibration curve (concentration range 0.5448–0.9080 µg mL^{-1}, $n = 3$, $R^2 = 0.9997$), the unknown concentrations were determined. The EE % was obtained applying the following equation (David et al., 2019 & Rehab et al., 2021):

$$EE\% = \frac{Total\ amount\ of\ AMP-BLF - Total\ amount\ of\ free\ AMP-BLF}{Total\ amount\ of\ AMP-BLF} \times 100 \quad (1)$$

the total amount of AMP-BLF is the real weighed quantity, and the total amount of free AMP-BLF is the quantity of AMP-BLF in the supernatant.

2.6.2. Measurements of particle size, distribution, and Zeta potential

Bidistilled water was used to dilute the thermosensitive gel containing the drug-loaded NPs (1 mL to a total volume of 10 mL), and a Zetasizer 3600 was used to determine particle size (PS) at 25 °C (Malvern Instruments, Malvern, U.K.) using the light scattering technique (DLS). The angle of light scattering was fixed at 90° and the range of laser obscuration was 10%–20%. Each sample was subjected to three cycles. ANOVA one-way statistical testing was used to examine whether there were any significant changes between formulae particle size and zeta potential (Rebecca and Rachael, 2013).

2.6.3. In-vitro release studies

In-vitro release of AMP and BLF from the thermosensitive gel containing the drug-loaded NPs was determined **by** employing a Bag dialysis approach (Desiree et al., 2019). Concisely, the dialysis membrane (typical molecular weight threshold of 14,000 Da; Sigma-Aldrich Co) was soaked overnight in the release medium (phosphate buffer saline solution (pH 7.4) with 25% ethanol to maintain the sink condition) (David et al., 2019). Then, the dialysis bag enclosing 2 mL (equivalent to 0.5 mg of AMP-BLF) of each formula or AMP-BLF suspension was placed in a 25 mL release medium in amber bottles. The bottles were then placed within a shaker working at 37 ± 0.5 °C and 100 rpm. In an effort to maintain sink condition, after taking 3 mL aliquots at predetermined intervals (0, 0.5, 1, 2, 4, 6, 8, 10, 12, 24 and 48 h), it was replaced with an equivalent volume of new release medium. Retention periods for AMP and BLF were calculated to be 4.3 and 11.1 min, respectively. The percentage released was determined using HPLC measurements at λ = 405 nm against the calibration curve ($R^2 = 0.9997$). The release profiles were fitted to the zero, initial, Higuchi diffusion, and Korsmeyer-Peppas models. The greatest coefficient (R2) indicates the most suitable model (Desiree et al., 2019).

2.6.4. Selection of the optimum formula

Using Design-Expert® software version 10 (Stat-Ease, Inc., Minneapolis, Minnesota, USA), numerical optimization was used to find desirable factors while disregarding non-significant ones. The Highest EE % and ZP (absolute value), *in-vitro* release (Q48h) > 80%, lowest PS and PDI were selected (Table 2). For further evaluation, the most desirable formula (near to 1) was used (David et al., 2019 & Rehab et al., 2018).

2.6.5. In-vitro characterization of the optimized formula (A-B1)

2.6.5.1. Drug polymer interaction using Fourier transform infrared (FT-IR) spectroscopy. Drug-polymer chemical interactions were studied by FTIR spectroscopy (Shimadzu 43,000 spectrophotometer, Kyoto, Japan). In brief, samples of the thermosensitive gel containing the drug-loaded NPs were prepared as a compact disc with KBr. Spectra were recorded at a scanning range of 4000–400 cm^{-1} and a mean spectrum of 32 scans at a resolution of 2 cm-^{1} was obtained (Rebecca and Rachael, 2013; Janagam et al., 2017; Berthomieu and Hienerwadel, 2009).

2.6.5.2. Differential scanning calorimetry (DSC) analysis. A Perkin-Elmer apparatus was used to perform the Differential Scanning Calorimetry (DSC) analysis. Samples (6.5–10 mg) were heated at a rate of 100 °C/min on an aluminum pan in a nitrogen environment at temperatures ranging from 0 to 400 °C. The DSC experiment was carried out using a nitrogen gas flow rate of 20 lb./in^2 (Montenegro et al., 2018).

2.6.5.3. Transmission electron microscopy (TEM). The morphology of the optimized formula of A-B1-NPs was studied with the use of a transmission electron microscope (TEM) (JEM-1230, Joel, Tokyo, Japan). Negatively stained with a 1% aqueous solution, samples were deposited on a carbon-coated grid surface before drying till visualization at room temperature (Malatesta, 2016 and Sammar et al., 2022).

2.6.5.4. Atomic force microscopy (AFM). Atomic force microscopy (AFM) was used on a Dimension Icon microscope (Bruker, Massachusetts, USA) to assess surface morphology and roughness. A glass slide with AMP-BLF-NPs taped to it was scanned in a tapping mode (2 m scan size, 0.894 Hz scan rate, 512 samples per line).

2.6.5.5. γ-Irradiation sterilization. To prevent any bacterial

Table 2
Composition and combination of the variously synthesized thermosensitive gel containing the drug-loaded NPs with associated values of response variables for determination of optimum formulation ($n = 3 \pm$ SD).

Trials*	Factors		Responses				
	A1: drug: PLGA ratio	A2: P407: P188 ratio	Y1:PS (nm) (Mean ± SD)	Y2: ZP (mV) (Mean ± SD)	Y3: PDI (Mean ± SD)	Y4:EE % (Mean ± SD)	Y5:Q48h % (Mean ± SD)
A1	1:2	1:5	410.0 ± 0.3	20.3 ± 0.5	0.09 ± 0.02	70.3 ± 0.3	75.0 ± 0.5
A2	1:2	1:10	510.0 ± 0.5	23.5 ± 0.5	0.10 ± 0.04	73.5 ± 0.4	71.0 ± 0.5
A3	1:2	1:15	601.0 ± 0.5	25.0 ± 0.5	0.08 ± 0.03	72.4 ± 0.5	79.0 ± 0.5
A4	1:5	1:5	250.0 ± 0.4	26.4 ± 0.5	0.07 ± 0.04	84.5 ± 0.5	81.0 ± 0.4
A5	1:5	1:10	230.0 ± 0.4	28.1 ± 0.5	0.07 ± 0.03	85.3 ± 0.5	82.0 ± 0.5
A6	**1:5**	**1:15**	**178.0 ± 0.6**	**31.2 ± 0.4**	**0.04 ± 0.01**	**92.3 ± 0.5**	**93.0 ± 0.6**
A7	1:10	1:5	384.0 ± 0.4	28.7 ± 0.4	0.09 ± 0.03	75.9 ± 0.5	85.0 ± 0.5
A8	1:10	1:10	430.0 ± 0.5	22.9 ± 0.4	0.08 ± 0.02	79.5 ± 0.5	73.0 ± 0.4
A9	1:10	1:15	450.0 ± 0.4	24.9 ± 0.5	0.08 ± 0.03	81.6 ± 0.4	79.0 ± 0.5
B1	1:2	1:5	350.0 ± 0.4	28.4 ± 0.5	0.12 ± 0.01	78.3 ± 0.5	83.0 ± 0.4
B2	1:2	1:10	320.0 ± 0.5	29.2 ± 0.6	0.12 ± 0.02	82.2 ± 0.5	84.0 ± 0.3
B3	**1:2**	**1:15**	**201.0 ± 0.5**	**32.5 ± 0.4**	**0.07 ± 0.01**	**91.2 ± 0.4**	**92.0 ± 0.5**
B4	1:5	1:15	550.0 ± 0.5	23.4 ± 0.3	0.19 ± 0.03	66.9 ± 0.5	64.0 ± 0.5
B5	1:5	1:5	444.0 ± 0.4	23.5 ± 0.5	0.14 ± 0.04	69.8 ± 0.3	73.0 ± 0.5
B6	1:5	1:10	450.0 ± 0.4	28.0 ± 0.5	0.20 ± 0.03	74.5 ± 0.5	80.0 ± 0.4
B7	1:10	1:15	481.0 ± 0.5	27.3 ± 0.4	0.18 ± 0.03	75.7 ± 0.5	79.0 ± 0.5
B8	1:10	1:5	501.0 ± 0.4	22.0 ± 0.3	0.13 ± 0.01	65.7 ± 0.4	60.0 ± 0.5
B9	1:10	1:10	540.0 ± 0.5	22.1 ± 0.6	0.19 ± 0.02	65.9 ± 0.3	63.0 ± 0.5
A-B1	**1:2**	**1:15**	**177.0 ± 0.3**	**31.9 ± 0.3**	**0.01 ± 0.01**	**90.8 ± 0.5**	**90.9 ± 0.5**
A-B2	1:5	1:15	210.0 ± 0.5	31.2 ± 0.3	0.02 ± 0.02	87.5 ± 0.5	87.0 ± 0.5

* All formulations contain constant amount of 100 mg PEI, 50 mg PEG, 5 mg EDC and 5 mg NHS.

contamination, AMP and BLF NPs were sterilized using γ- irradiation source (Aragogamma, Barcelona, Spain) dose of 25 kGy at 60 °C. This dosage is sufficient to sterilize pharmaceutical items when bioburden is unknown, in accordance with the European Pharmacopeia, retaining a sterility assurance level (SAL) (Raghavendra et al., 2008).

2.6.5.6. Short-term Stability of nanoparticles. For three months, the optimized formula nanoparticles were kept at 4 °C and 25 °C, respectively. Samples were then taken, and the mean PS, and ZP (measured using a Zeta-sizer Nano ZS from Malvern Instruments Ltd., Malvern, UK), EE%, PDI, and Q48h were assessed. The trials were done in triplicate, and GraphPad Instate version 3 software (GraphPad Instate Software, Inc. USA) was used for performing *t*-test to point out the potential statistical difference (Raghavendra et al., 2008).

2.6.5.7. Determination of the sol-gel transition temperature. The sol-gel transition temperature was calculated using a prior methodology (Mohamed et al., 2022). The method was executed by pouring 2 mL of the gel into a closed tube vial and heating in a water bath at 20 °C. Every 1 °C increase in temperature was followed by a 90° rotation of the vials until the bath reached 65 °C. $T_{sol\text{-}gel}$, or the temperature at which the gel did not flow while the vial was rotated, was calculated. Three runs of the test were executed.

2.6.5.8. In-vitro anti-fungal activity Study of the thermosensitive gel containing the drug-loaded NPs

2.6.5.8.1. Agar disc diffusion method. The anti-fungal activity of the thermosensitive gel containing AMP-loaded PLGA-PEG-PEI NPs and AMP-BLF-loaded PLGA-PEG-PEI NPs was tested using the agar disc diffusion technique according to the committee for Clinical Laboratory Standards (NCCLS) (Bancroft and Turner, 2013). Fungal strain suspensions were prepared, and the turbidity was adjusted to obtain a final concentration to match that of a 0.5 McFarland using a spectrophotometer at 530 nm. A sterile disc loaded with 0.1 mL of each drug formulation at a concentration equivalent to 200 g/100 L of AMP-BLF NPs (0.2%*w/v*) was added to the surface of potato Dextrose agar plates pre-inoculated with fungal strain. AMP-BLF solution was used as a blank; Ketoconazole discs were used as a control. Before incubation at 37 °C for 24–48 h, the plates were left for 30 min to enable diffusion. The diameter of inhibition zones around the wells was measured in millimeters (Calliandra et al., 2018).

2.6.5.8.2. Determination of minimum inhibitory concentration (MIC). Clinical and Laboratory Standards Institute (CLSI) broth microdilution method was used to determine the lowest inhibitory concentration for the thermosensitive gel containing AMP-loaded PLGA-PEG-PEI NPs, BLF-loaded PLGA-PEG-PEI NPs and AMP-BLF loaded PLGA-PEG-PEI-NPs against the tested fungal strains (S'anchez-L'opez et al., 2016). The concentration range tested was 0.031–16 μg/mL and 100–256 μg/mL for AMP and BLF respectively. Briefly, 50 μL of two-fold serial dilutions of the drug formulations originally dissolved in 50 L dimethyl sulfoxide (DMSO) was prepared. The prepared doses were placed in the 96 wells microplate, which contained 100 μL of Sabouraud Dextrose broth. Each well received a volume of 50 μL of fungal suspension with an approximate concentration of 10^6 mL^{-1}. The microplate was incubated for 48 h at 28 °C. At the maximum level of dilution, the lowest inhibitory concentration was attained, with no fungal growth as a consequence. MIC measurement was done in triplicate to ensure results.

2.7. Ex-Vivo study

2.7.1. EX-Vivo corneal permeation study

The corneas of male New Zealand rabbits (2.5–3.0 kg) were used to investigate *ex-vivo* AMP and BLF permeation from AMP-NPs, BLF-NPs, and their combinations, in conformity with the University of Cairo's Ethics Committee of Animal Experimentation and under the supervision of a veterinarian. The animals were given intramuscular ketamine hydrochloride (35 mg/kg) and xylazine (5 mg/kg) anesthesia before being terminated with sodium pentobarbital (100 mg/kg) overdose given through the marginal ear vein under deep anesthesia (Rehab et al., 2021& Gonzalez-Pizarro et al., 2018). Eyes were extracted, dissected, and sent to the laboratory in an artificial tear solution. Franz cells having a 0.64 cm^2 diffusion space between the donor and receptor compartments, were fixed with the corneas. In all studies, 2 mL samples of the test formulations (AMP-NPs, BLF-NPs and AMP-BLF-NPs) in thermosensitive gel were incubated in donor compartments and covered quickly to prevent evaporation. Phosphate-buffered saline (PBS) and 25% ethanol was used to fill receptor compartments, which were magnetically agitated and maintained at a temperature of (37 °C). For 6

h, a 300 μL sample was removed from the receptor compartment and replaced with an equal amount of new receptor media at predetermined intervals. Throughout the experiment, the sink conditions were maintained. The total quantity of AMP and BLF penetrated was calculated from the amount of AMP and BLF in the receptor medium at each time point and displayed as a function of time (G'omez-Segura et al., 2020). RP-HPLC was used to examine the samples (Desiree et al., 2019; David et al., 2019). The values were given as the mean and standard deviation of triplicates. The total AMP and BLF readings were plotted *vs.* time to calculate permeation parameters and estimate the x-intercept using linear regression analysis (Julia et al., 2000). The permeability coefficient (Kp) (cm/h) (Eq. 2), steady-state flux (J) (μg/cm^2/h), and amount penetrated after 48 h (Q48) (g) was calculated.

$$Kp = J/C_0 \quad (2)$$

where C_0 is the starting drug concentration (μg/cm^3) and J is the steady state flux considered as the slope of the linear part (μg/cm^2/h).

The amount of drugs retained inside the tissue (QR) was determined after the recovery of the corneal sample. The tissue was weighed, rinsed in distilled water, and sonicated for 1 h in MQ® water in an ultrasonic bath. The values were given as the mean and standard deviation of triplicates.

2.7.2. Confocal laser scanning microscopy study (CLSM)

The formulas were created as before, with the exception that AMP-BLF was eliminated and 1% (*w/v*) Fluorescein diacetate (FDA) was added to the aqueous phase. The goal of this study was to determine the infiltration of the optimized AMP-BLF NPs throughout several layers of the cornea (Desiree et al., 2019& David et al., 2019). In diffusion chambers akin to those used in the earlier *ex-vivo* permeation experiment, bovine corneas were fixed. PLGA-PEG-PEI was applied to the surface of the cornea for 10 h in order to replicate the administration of the optimized formulas in contact with the surface of the eye. Through longitudinal slices that were embedded in paraffin wax and divided into many sections using a microtome (Rotary Leica RM2245; Leica Biosystems, Wetzlar, Germany), the fluorescence in the corneal tissue was identified. The slide was seen using an inverted microscope (LSM 710; Carl Zeiss, Oberkochen, Germany). The maximum wavelengths of FDA excitation and emission were 497 nm and 516 nm, respectively. LSM Image gave the confocal images. Release 4.2 of the browser software from Jena, Germany's Carl Zeiss Microimaging GmbH was employed (Elsayed and Sayed, 2017). Different parts of the corneal tissues were chosen for comparative assessment between the optimized AMP-BLF NPs and AMP-BLF solution and light intensity was measured. Applying the Student's *t*-test with GraphPad Instat version 3 software (GraphPad Instat Software, Inc. USA), potential significant difference at ($P < 0.05$) was determined. Three trials were conducted in the experiment.

2.8. Cell culture assays

2.8.1. Cytotoxicity assays

In-vitro cytotoxicity tests were performed on human corneal epithelial cells (HCE-2). HCE-2 cells appear to be an ideal model for AMP-NPs and BLF-NPs for ocular delivery. HCE-2 cells were cultured in a serum-free keratinocyte medium. It contained insulin (0.005 mg/mL), bovine serum (10% *v/v*), hydrocortisone (500 ng/mL), penicillin (100 ng/mL), and streptomycin (100 mg/mL). It was enriched with 0.05 mg/mL bovine pituitary extract and 5 ng/mL epidermal growth factor. It was determined to cultivate cells to 80% confluence in a humidified 10% CO_2 atmosphere at 37 °C in a culture flask. MTT (Bromide of 3-(4,5-dimethyl-2-thiazolyl)-2,5-diphenyltetrazole) was utilized as a cell viability indicator in HCE-2 corneal cell line viability experiments. After 24 h of incubation at 37 °C, cells were transferred to a 96-well plate and treated with AMP-NPs, BLF-NPs, and AMP-BLF solution at various drug doses (0.04–0.1 mg/mL). After twenty-four hours, the cells were washed with PBS and incubated for two hours in a fresh medium containing 0.25% MTT. After removing the media, DMSO was employed to lyse the cells. Cells' $\lambda = 560$ nm absorbance was measured *via* an automated Modulus TM microplate reader (Turner BioSystems, CA, USA). The MTT assay results were expressed as a percentage decrease in comparison to untreated (control) cells (Rehab et al., 2021).

2.8.2. Determination of proinflammatory cytokines

Using HCE-2 (1×10^5 cells /mL) cells seeded in 12-well plates, the anti-inflammatory activity of the NPs was assessed. Inflammation was induced with lipopolysaccharide (LPS) (1 μg/mL). After that, drug-loaded NPs were put into the culture medium at 0.2 mg/mL (drug concentration). The positive control consisted of cells that had only been stimulated with LPS, whereas the negative control consisted of cells that had not been activated at all. The supernatants were collected after 24 h and centrifuged at 4 °C for 10 min at 16000 g before being kept at −80 °C until use. ELISA kits (B.D. Biosciences, CA, USA) were used to measure unknown amounts of the proinflammatory cytokine interleukin 8 (IL-8) and tumor necrosis factor (TNF-α) according to the manufacturer's recommendations.

2.9. In-vivo study

2.9.1. Preparation of animals

All rabbits were sedated in the operation room with an intramuscular injection of 1 mL (50 mg/mL) of Ketamine (Ketalar®). To provide topical anesthesia, rabbits had benoxinate eye drops injected into their conjunctival sacs. All rabbits' right corneas were marked with a 7 mm corneal trephine, the epithelium was scraped away, and then fungal strain was injected. The posterior corneal stroma was injected with a 27-gauge needle (Bancroft and Turner, 2013). The entire surgery was performed under strict aseptic conditions, using a binocular microscope and chloramphenicol eye drops to clean the eyes.

To confirm the organism's flourishing, all corneas were inspected for symptoms of infection 48 h later. After that, the rabbits were separated into five groups and given codes and numbers, with each group's right eye getting a different treatment.

Each group designated to get AMP-NPs, BLF-NPs, AMP-BLF-NPs, AMP-BLF solution, and Ketoconazole, received 200 mg/day of the respective treatment. The left eye served as a control in all cases, receiving an identical amount of saline solution. The formulation was applied to the rabbit's cornea three times each day for two weeks. An identical process was employed for *Candida albicans, Fusarium, and Aspergillus flavus*. Every day, each rabbit was followed up using a written sheet following the enumeration system.

From the beginning of the infection through the end of therapy, photos were collected for documentation. Rabbits were slain two weeks later, and corneas were dissected at the limbus and submitted for pathological testing in a 10% formaldehyde solution to determine if the fungus was present and the extent of inflammation for each formula. After the study, the rabbits' bodies and remains were frozen and delivered to the veterinary medicine laboratory, where they were burned following a common protocol.

2.9.2. Ocular irritancy test (Draize test)

The purpose of this test was to confirm the formula's safety. By noting any redness, discomfort, or increased tear production after application to the eyes of albino rabbits, any potential optical irritancy and/or harmful effects of the optimal formulation were assessed. Three albino rabbits were used in the test. For the experiment, the tested substance (optimal thermosensitive gel containing the drug-loaded NPs) was injected into only one eye, while the other eye worked normally.

2.9.3. Inflammation treatment

Using male New Zealand albino rabbits ($n = 6$ per group), the anti-inflammatory effect of BLF-NPs was compared to protein-free NPs and a control group that had received NaCl (0.9%). The right eye was

administered 50 µL of Sodium arachidonate (SA, 0.5%) dissolved in PBS, whereas the left eye acted as a control. Following 30 min of exposure, 50 µL of each treatment was administered. The Draize-modified scoring system was used to assess inflammation three hours after the treatments were administered (Chen et al., 2019 & Diaz-Garrido et al., 2019).

2.9.4. *In-vivo corneal histopathological examination*

Corneas from slain animals were cut at the limbus and submitted to the pathology lab in 10% formaldehyde solution under complete aseptic circumstances to assess the presence or absence of the fungus and the level of inflammation for each formula. Hematoxylin and eosin were used to stain the slides for each specimen (H&E). All H&*E*-stained slides were investigated under a light microscope to determine the severity of the inflammatory reaction and the presence or absence of fungal spores (Rebecca and Rachael, 2013; Seyfoddin and Al-Kassas, 2013).

3. Results and discussion

All Formulations prepared from triblock polymers PLGA-PEG-PEI loaded NPs were used with P188/P407 thermosensitive hydrogel to enhance nanoparticles membrane rigidity, improve ability of the polymers to cement the leaky gap in the bilayer membranes, and give sustained drug release hydrogel with the goal of increasing the potency and effectiveness of the combination.

3.1. *In-vitro evaluation of PS, PDI, ZP, EE%, and Q48h of AMP and BLF formulas*

The response parameters and surface study results are shown in Table 2 and Fig. 2a, and b, respectively. AMP, and BLF concentration influence the PZ, PDI, and EE%. AMP increases encapsulation and reduces particle size and polydispersity index with a ratio of 1:5 for AMP to PLGA and 1:2 for BLF to PLGA embedded in 1:15 of P407:P188. For AMP, EE% of 84–92%, PS of 178–250 nm and PDI of 0.035–0.074 were achieved at the aforementioned ratios. For BLF, the used ratios achieved EE% of 78–91%, PS of 350–201 nm and PDI of 0.012–0.071. When a combination of both drugs (AMP-BLF) was used at a ratio of 1:2 of the mixture to PLGA and 1:15 of P407:P188, a high EE% (90.81 ± 0.54) was

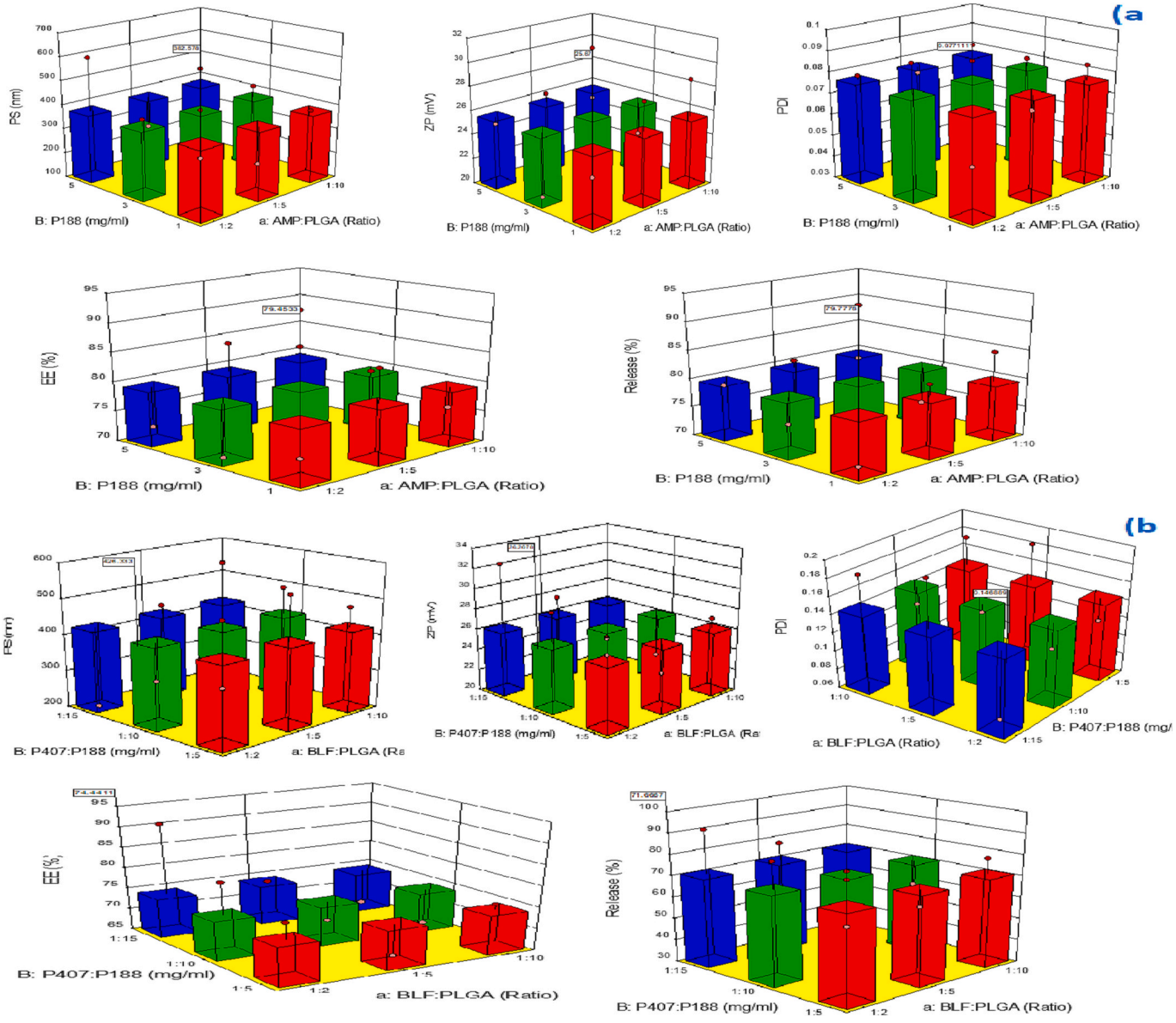

Fig. 2. Response 3D plots for the effect of (a) Drug A (AMP)&(b) Drug B (BLF): PLGA (X1) and P407:P188 (X2) on (a) EE%, (b) PS, (c) PDI, (d) ZP, and Drug release Q48 h of the formulations.

established.

BLF has a high molecular weight (3125.8 g/mol) compared to AMP (924.079 g/mol), which explains the higher maximum capacity for AMP (1:5) compared with that of BLF (1:2). At high ratio (1:15) of P407: P188 concentrations, optimal PDI values were found (<0.01), which is indicative of a monodispersed system. The tendency of AMP-BLF-NPs to form a positive charge on the surface can be ascribed to absorption processes taking place on the surface of the polymeric material. It is feasible that the surfactant is stationed around the NPs on the surface. Accordingly, raising the concentration of the surfactant is anticipated to saturate the surface of the NPs, hence increasing their PDI and average PS (Masoudipour et al., 2017). Appearance of the polymeric NPs can be altered from smooth to somewhat rough (as shown in Fig. 3) owing to absorption of the surfactant.

Due to ionization of carboxylic end groups on the polymer's surface, the utilized PLGA has a negative ZP. However, existence of the surfactant P188 has been reported to reduce the surface charge of the particles (Vega et al., 2012). Surface bonding of hydrophobic poly-oxy-propylene chains to the NPs takes place, while protrusion of the hydrophilic poly-oxy-propylene chains in the surrounding media helps conceal the surface negative charge formed on the NPs. In addition to the surfactant, the positive charge on the active moieties to be encapsulated (AMP, BLF) contributes to the covering of the negative charge of the polymeric material and yields a highly positive ZP of roughly +30 mV. Residence duration on the epithelium of the cornea increases in presence of a positive charge, which facilitates drug permeation and produces prolonged release (Andr'es-Guerrero et al., 2017). In this study, selection of the optimum formulation was based primarily on the values (percent) of EE and homogeneity of the samples (PS, PDI).

Using a direct dialysis bag approach, AMP and BLF *in-vitro* release when encapsulated in AMP-BLF-Triblock polymer as well as the *in-vitro* release of free AMP and BLF were determined. Release of AMP and BLF from NPs demonstrated a sustained and regulated pattern as shown in the cumulative drug release profiles in Fig. 4. Because of the weak link between the drugs and the surface of the NPs, release of AMP and BLF occurs faster within the first 10 h from the NPs than from free medicines (Carvajal-Vidal et al., 2019). Subsequently, the rate of drug release reduces dramatically, resulting in a steady release (92% after 48 h) that never reaches a plateau. Typically, polymeric matrices composed of PLGA-PEG-PEI exhibit characteristic release profiles with zero-order initial burst and subsequent slower release mediated *via* several mechanisms such as diffusion, erosion, or a combination of both mechanisms (Cano et al., 2018; Fu and Kao, 2010; S'anchez-L'opez et al., 2016).

To establish a kinetically sound model that best describes the release of AMP and BLF, the most prevalent kinetic models shown in Table 3 were run on the release data. The best model for adjusting the NPs formulation was the Korsmeyer-Peppas model (r^2 = 0.99, Akaike information criterion (AIC) = 50.12).

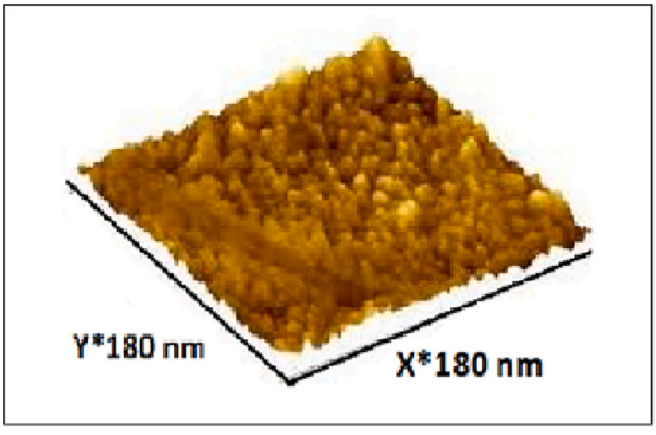

Fig. 3. 3D Atomic force microscopy (AFM) surface morphology of AMP-BLF loaded PLGA-PEG-PEI NPs.

3.2. In-vitro evaluation of the optimized formula

3.2.1. Fourier Transform infrared (FT-IR) spectroscopy

To examine drug-excipient interactions, FTIR spectroscopy was employed. The FTIR analysis results depicting the interaction of AMP, BLF, and PLGA-PEG-PEI are shown in Fig. 1S. There was no indication of a covalent bond formation between AMP, BLF, and PLGA-PEG-PEI. Among the prominent peaks in the IR spectra are the stretching vibrations of amide I (C = O and C—N) at 1638 cm^{-1} and amide II (N—H bending with contribution from C—N stretching vibrations) at 1520 cm^{-1}. O—H stretching vibration in water at 3279 cm^{-1} show the presence of residual H_2O. Methylene stretching, polyene C = C, C = O asymmetric stretches of amide VI in AMP molecule may be responsible for the peaks at 3420, 2926, 1560, 1070, and 510 cm^{-1}. In the PLGA triblock polymer analysis, the stretching vibration of the carbonyl group produced a notable band at 1750 cm^{-1}. The weak peaks represent the stretching vibrations of alkanes at 2956 cm^{-1}, whereas the stretching vibrations of C—O, and C–O–O are represented by the medium peaks at 1159 and 1088 cm^{-1}, respectively. P188 features two significant peaks, one at 2874 cm-1 for C—H stretching vibrations and the other at 1096 cm^{-1} for C—O stretching vibrations (Ghobad et al., 2021; Avinash et al., 2018).

AMP-NPs and BLF-NPs have profiles similar to PLGA-PEG-PEI, with the addition of peaks characterized by modest intensity owing to amide I, II, IV, and O—H vibrations in BLF molecule. The combinatory formula (A-B2-PLGA-PEG-PEI) demonstrates no chemical interactions between AMP, BLF, and the excipients.

3.2.2. Differential scanning calorimetry (DSC) analysis

Drug physical state inside NPs framework has a significant impact on the active material's release in both *in-vitro* and *in-vivo* experiments. DSC examinations were conducted in which the thermograms of AMP, BLF, PEG, PLGA, PEI, and the combination of AMP-BLF NPs were determined and shown in Fig. 2S. The thermogram of AMP and BLF reveals a sudden endothermic accident, with a maximum temperature (T_{max}) of 170.41 °C, linked with fusion event. Interestingly, the aforementioned accident was not recorded in the thermogram of BLF-NPs. This evidence suggests enclosure of BLF inside the polymeric matrix in the form of solid solution or molecular dispersion (Cano et al., 2019). The melting of AMP caused a peak in its thermogram at 172.98 °C. Because of the colligative capabilities, the melting point of AMP is reduced in all physical mixes. The significant reduction in the melting enthalpy of fusion in all NPs compared to the physical mixture indicates presence of intermolecular hydrogen bonds and medication's interaction with polymers. The results revealed that the increased melting point of AMP-BLF-PLGA-NPs was connected to functional group augmentation and hydrogen bonding reinforcing impact. Because of the improved solubility of the active drug, amorphous combination NPs may be advantageous (Thi et al., 2021).

3.2.3. Morphology and transmission electron microscopy (TEM)

The morphometric characteristics of the improved formulation of AMP-BLF-loaded-NPs were determined using TEM imaging and the pictures are shown in Fig. 5**.** Images revealed NPs with fairly spherical shapes and average particle sizes similar to those reported in PCS morphometry studies.

3.2.4. γ-irradiation effect of best formula A-B1 loaded PLGA-PEG-PEI NPs

γ–Irradiation was applied to the best formulation of A-B1-NPs for sterilization before being supplied as eye drops. Analysis was then conducted to assure that the irradiation had no effect on the properties of the system. According to the results shown in Table 4, irradiation did not affect the physicochemical parameters of the optimized NPs. There

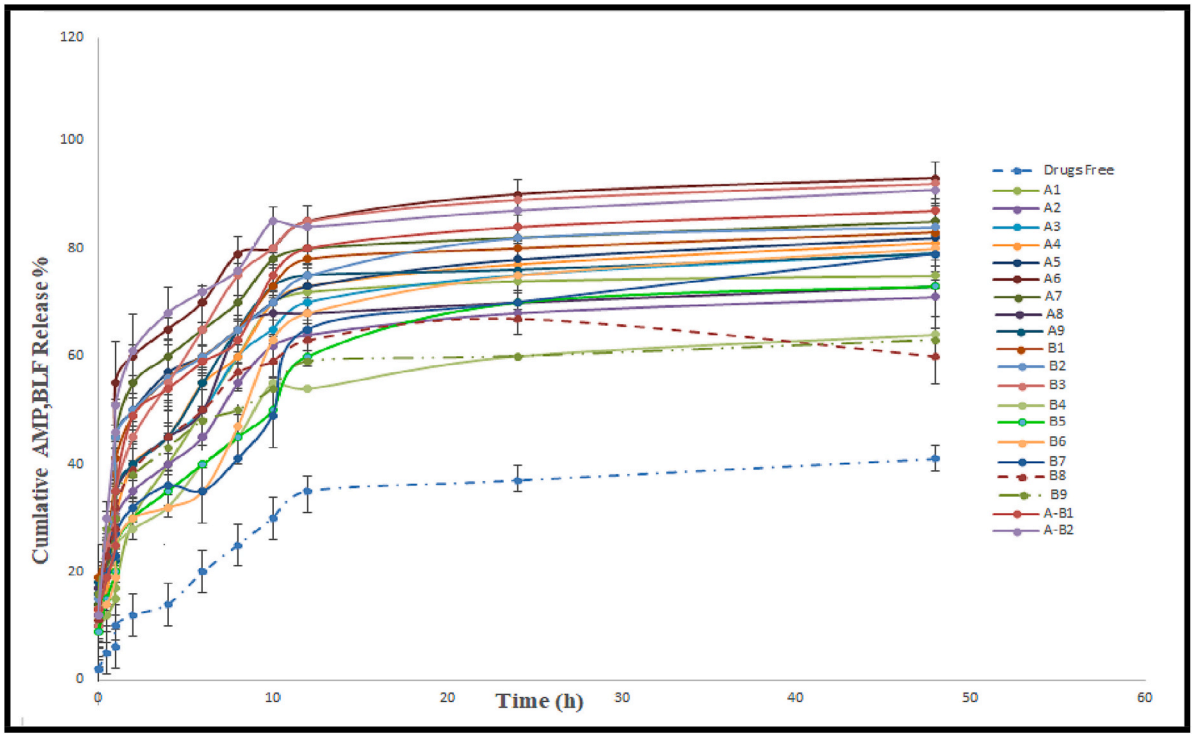

Fig. 4. The *in-vitro* release profiles of thermosensitive gel containing AMP-BLF-NPs compared to AMP-BLF Solution at 37 ± 0.5 °C, $n = 3 \pm$ SD.

Table 3
Kinetics of AMP-BLF *in-vitro* release from thermosensitive gel containing NPs and drug solution.

Models	AMP-BLF-NPs (A-B1)	R^2	AMP-BLF Solution	R^2
Zero Order	91.2	0.18	99.9	0.62
First Order	82.4	0.75	79.6	0.65
Higuchi	79.9	0.62	81.2	0.71
Kors Meyer - Pappas	50.2	0.99	79.0	0.82

were no statistically significant changes between the NPs before and after sterilization. As a result, these modest changes do not influence the therapeutic properties of A-B1-NPs (Tapia-Guerrero et al., 2020; Rehab et al., 2021).

3.2.5. *Short-term stability of nanoparticles*

The stored vesicles did not aggregate or exhibit any physical alterations at the end of the experiment. Table 5 shows the values of EE%, PS, PDI, ZP, and Q48h when the optimized formula was fresh and stored at 4 °C and 25 °C (3 months). In EE%, PS, ZP, and Q48h, marginal changes ($p > 0.05$) were discovered. This result emphasizes the formula's great stability. The large positive charge of the optimum formula averts stored NPs' aggregation/agglomeration. A large surface area would also be

Table 4
Entrapment efficiency of best formula (A-B1) and physicochemical properties before and after sterilization (A-B1 25 kGy).

Parameters	A-B1 freshly prepared	A-B1 25 kGy after gamma radiation
PS (nm)	177.0 ± 0.3	176.0 ± 0.3
ZP (mV)	31.9 ± 0.3	31.0 ± 0.3
PDI	0.011 ± 0.01	0.010 ± 0.01
EE%	90.8 ± 0.6	89.2 ± 0.3
Q48 h	90.9 ± 0.5	90.0 ± 0.2

Table 5
Effect of short-term storage on the physicochemical properties of the best formula (A-B1).

Parameters	A-B1 freshly prepared	A-B1 after 3 months of storage at 4 °C	A-B1 after 3 months of storage at 25 °C
PS (nm)	177.0 ± 0.3	174.0 ± 0.3	173.0 ± 0.4
ZP (mV)	31.9 ± 0.3	29.0 ± 0.4	30.0 ± 0.4
PDI	0.011 ± 0.01	0.010 ± 0.01	0.010 ± 0.01
EE%	90.8 ± 0.6	89.7 ± 0.3	89.2 ± 0.2
Q48h	90.9 ± 0.5	90.0 ± 0.5	89.0 ± 0.3

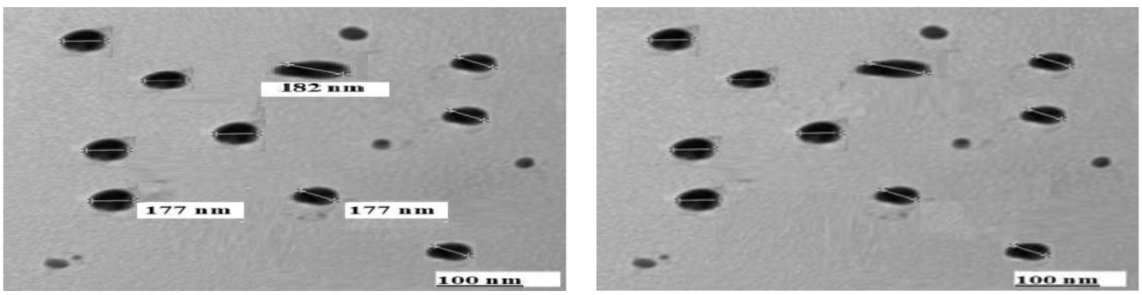

Fig. 5. Transmission electron microscope (TEM) pictures of the thermosensitive gel containing AMP-BLF-loaded NPs.

created by the optimal formula's small PS, allowing the ionizable surface groups on the NPs to expose their charge. After 1, 15, 30 days, and 3 months at 4^0 and 25 °C, the improved formulation was assessed. Turbiscan® Lab was utilized for determination of destabilizing processes which influence particle speed and size, as shown in Fig. 6. Particle migration to the cell's upper section reduces the lower part's concentration. This decreases the backscattering signal (negative peak). Backscatter profiles with a 5% deviation don't show significant particle size differences. 10% variations imply formulation instability (Elsayed and Sayed, 2017).

3.2.6. *Determination of the Sol–Gel transition Temperature*

One of the crucial factors in the formulation of thermosensitive gels is the gelation temperature as the gel must stay liquid at room temperature in order to give the exact dosage (Mohamed et al., 2022). Visual inspection revealed that the liquid dispersion of A-B1 and A-B2 was clear at room temperature. The eye mucosal layer is said to have an average temperature of 34 °C. Imitating the circumstances of the human eye, the formulations A-B1 and A-B2 demonstrated sol-gel transition at 34 °C. This suggests that when A-B1 and A-B2 come into touch with the environment of the eye, they may produce a viscoelastic gel.

3.3. *Ex-vivo corneal permeation*

To assess, compare and calculate different penetration parameters of the thermosensitive gel containing AMP-BLF-NPs and free AMP-BLF across the cornea, an *ex-vivo* permeation study was conducted and the results are shown in Fig. 7 and Table 6**.** Apart from AMP-BLF QR values; the AMP-BLF-NPs formulation demonstrated remarkable superiority ($p < 0.05$) in all evaluated permeation parameters compared to free AMP-BLF. AMP-BLF when encapsulated within the NPs, enters the cornea more quickly than from ABP-BLF solution, as evidenced by J value for AMP-BLF-NPS that is almost twice that for free ABP-BLF. This is because polymers have higher lipophilicity than free proteins. The cornea's epithelial layer is made of lipid, preventing hydrophilic molecules from entering and serving as a rate-limiting barrier for ocular-level medication delivery (Soni et al., 2019). The other permeation measures reveal close ratio, with AMP-BLF-NPs having a higher Kp and Q48h than free AMP-BLF. NPs therefore promote AMP-BLF action on the cornea and deeper on the aqueous humor (Shengtao et al., 2018). Aside from that, changes in the AMP-BLF QR between formulations were not significant. After applying the NPs formulation, the quantity of drug retained in the corneal tissue is a function of the fraction of AMP-BLF that is not encapsulated and the fraction undergoing first burst ejection from the AMP-BLF that is weakly attached to the NPs surface (Marcelle et al., 2018). By gentle releasing of AMP-BLF throughout the corneal tissue, the NP formulation may efficiently distribute the medicine to the proper place, making it useful for treating ocular fungus and Inflammation caused by allergies, trauma, or fungal infection.

3.4. *Confocal laser scanning microscopy (CLSM)*

CLSM manifested penetration potency across the corneal layer after utilizing FDA incorporated in the selected AMP-BLF-NPs instead of AMP

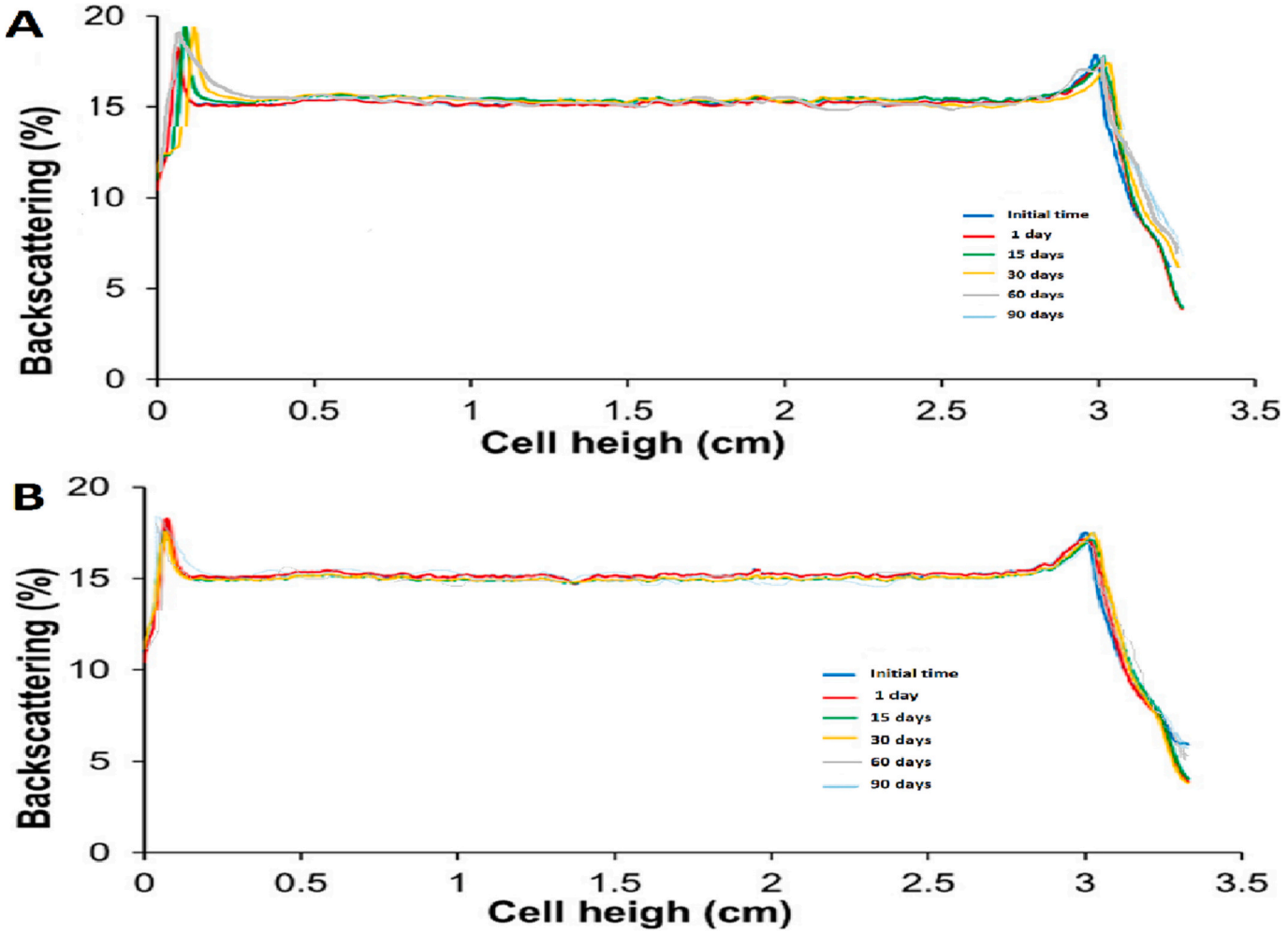

Fig. 6. Backscattering profiles of the thermosensitive gel containing AMP-BLF NPs stored at: (**A**) 4 °C and (**B**) 25 °C.

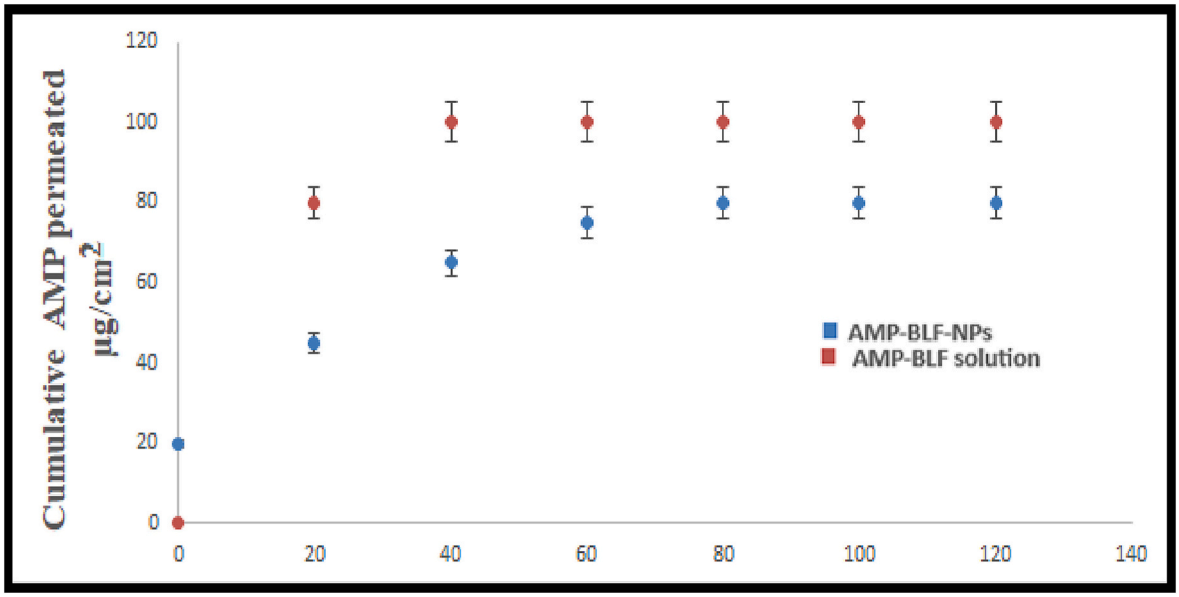

Fig. 7. AMP-BLF-NPs thermosensitive gel *ex-vivo* corneal penetration profile compared to AMP-BLF solution.

Table 6
Ex-vivo pharmacokinetic parameters of the AMP-BLF-NPs thermosensitive gel *ex-vivo* corneal permeability *versus* AMP-BLF solution estimated by linear regression.

Parameters	AMP-BLF-NPs	AMP-BLF solution
J ($\mu g \cdot h^{-1} \cdot cm^{-2}$)*	100.05 ± 0.1	57.1 ± 0.1
Kp · 10^3 ($cm \cdot h^{-1}$)*	10.01 ± 0.03	5.7 ± 0.2
Q48h (µg)*	1884.2% ±0.1	945.4 ± 0.1
QR ($\mu g \cdot g^{-1} \cdot cm^{-2}$)	0.9 ± 0.01	1.1 ± 0.01

* $p < 0.5$ for statistical significance.

and BLF solution. The intensity of fluorescent light was measured after ocular delivery and the results are displayed in Fig. 8. The depth of NPs' penetration through the corneal tissues was determined by performing scans of the longitudinal section. The NPs' preparation was able to penetrate deeply into corneal layers, as evidenced by homogenously distributed fluorescence with high and great intensity. The small size, which provides large surface area, and the presence of PLGA as a permeability enhancer, explain the observed deep penetration of the NPs. Nonetheless, quantifying the maximum intensity of the fluorescent light, with and without nanoparticles, ascertains that the existence of triblock polymer vesicles augments the penetration of the drugs. This finding assures that NP formulation can effectively deliver the medications to the correct location, making it suitable for treating ocular fungus and inflammation.

Anti-fungal activity evaluation was assessed using the agar disc diffusion method and MIC was determined. The results revealed *that Candida albicans, Fusarium, and Aspergillus Flavus* were highly sensitive to AMP in A1-NPs and AMP in A-B1-NPs as compared to ketoconazole at low dosages, as shown in Table 7 and graphically in Fig. 9**.** Anti-fungal activity of the A-B1-NPs formulation was significantly higher than that of A1-NPs formulation against all tested strains, where larger inhibition zones were produced.

The MIC values of A1-NPs formulation against *Candida albicans, Fusarium, and Aspergillus flavus* were 14 µg /mL, 16 µg /mL, and 17 µg /mL, respectively. In contrast, The MIC values of A-B1-NPs formulation were 4 µg/mL, 4 µg/mL, and 6 µg/mL, respectively. Presumably, the properties of the NPs, such as PS, PDI, and ZP, have profoundly impacted the activity of the tested formulations against different fungal strains. Nevertheless, augmented permeation of AMP from the optimum formulation (A-B1-NPs) allows the loaded drug to contribute higher antifungal activity, which leads to lower MIC value as compared with A1-NPs.

3.5. *Evaluation of in-vivo microbiological activity*

3.5.1. *Visual Evaluation of the possibility of ocular discomfort in the optimized thermosensitive gel containing A-B1-NPs formula*

In-vivo testing data in Fig. 3S show no evidence of inflammation or corneal, conjunctival, or iris injury. Edema of the conjunctiva and drainage were always graded zero. At all observations, the scores for iris hyperemia and corneal opacity were zero. As a consequence for absence of *in-vivo* irritating effects, the A-B1 loaded NPs have the possibility to be

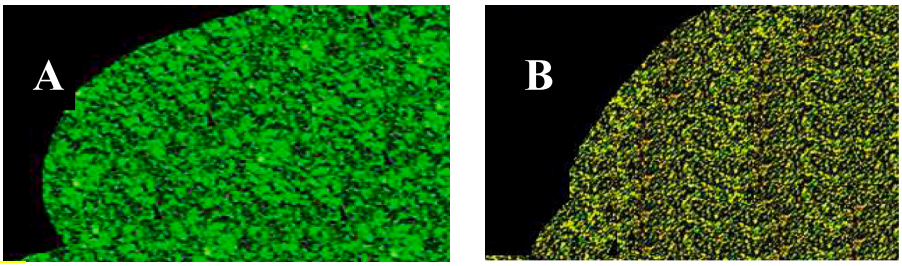

Fig. 8. Confocal laser microscope photomicrograph of a longitudinal section in bovine cornea treated with thermosensitive gel containing AMP-BLF-NPs (A), and AMP-BLF solution (B).3.4. *In-vitro anti-fungal activity evaluation of the thermosensitive gel containing AMP Loaded PLGA-PEG-PEI-NPs* and and *AMP-BLF-Loaded PLGA-PEG-PEI -NPs.*

Table 7
In-vitro anti-fungal susceptibility of the thermosensitive gel containing A1-NPs or A-B1-NPs, A-B1 solution, and Ketoconazole (control) ($n = 3 \pm$ SD).

Fungal Strains	Item under Test	Diameter of Zone in (mm) (mean ± SD)	MIC (μg/mL) (mean ± SD)
	A1-NPs	18.0 ± 0.4	14.0 ± 0.9
Candida albicans	A-B1-NPs	21.0 ± 0.1	4.0 ± 0.1
(RCMB 005003)	A-B1 solution	15.8 ± 0.4	3.4 ± 0.5
	Ketoconazole	14.0 ± 0.6	2.6 ± 0.3
	A1-NPs	19.0 ± 0.5	16.0 ± 1.0
Fusarium	A-B1-NPs	20.0 ± 0.7	4.0 ± 0.2
(RCMB 080352)	A-B1 solution	14.2 ± 0.2	2.5 ± 0.2
	Ketoconazole	14.0 ± 0.6	2.4 ± 0.4
	A1-NPs	16.0 ± 0.3	17.0 ± 1.05
Aspergillus flavus	A-B1-NPs	20.0 ± 0.5	6.0 ± 0.4
(RCMB 002002)	A-B1 solution	12.0 ± 0.3	3.2 ± 0.3
	Ketoconazole	12.0 ± 0.2	2.9 ± 0.5

of therapeutic interest.

3.5.2. *In-vivo activity study*

Five groups of rabbits were employed to investigate the impact on each of the three fungal infections (*Candida albicans, Fusarium, and Aspergillus flavus*). In all cases, the control was the left eye. Group 1 was treated with A1-NPs, Group2 with B1-NPs, Group 3 with A-B1-NPs, Group 4 with A-B1 solution and Group 5 with Ketoconazole. The medication was administered 48 h after the inoculation to allow for the appearance of fungal keratitis, which was validated by clinical inspection of the corneas. Photographs, Fig. 10 **(A-F),** were collected to document fungal keratitis (infiltration, ciliary injection, and hypopyon) caused by *Candida albicans, Fusarium, and Aspergillus flavus* infection, in the five treatment groups. In terms of the extent and depth of corneal invasion, rabbits treated with the A-B1-NPs formula fared better than rabbits treated with A1-NPs, B1-NPs, and A-B1 solution. This finding observation could be explained in the light of the fact that A-B1-NPs had greater potential for synergistic effect against fungal infection along with its associated inflammation, owing to coexistence of AMP, as antifungal agent, and BLF, as anti-inflammatory and anti-dry eye agent. Moreover, the polymeric matrix's preservation, delayed and sustained release of AMP and BLF may enhance corneal permeability, creating an anti-fungal and anti-inflammatory activity that lasts longer. Polymeric nanostructured an systems improve drug's availability to the ocular tissues, particularly at the level of the cornea and deeper tissues, such as the vitreous fluid and the retina. This is imperative for effective therapy of fungal infections and inflammation (Katrien et al., 2020; Zhen et al., 2021).

3.6. *Cell culture assays*

3.6.1. *Cytotoxicity of nanoparticles*

HCE-2 cells were used to test the safety of A-B1-NPs. Fig. 11 shows the results. A-B1-NPs had no cytotoxic effects after 24 h of incubation for concentrations up to 420 μg/mL. The vitality of cells was >85%. Therefore, it can be concluded that A-B1-solution had no cytotoxic effects at any concentration tested. Lactoferrin is found in healthy tear fluid and plays a significant role in iron retention, which contributes to defense against infections and minimization of oxidative stress. Making up to 20–30% of total proteins in healthy humans, tear lactoferrin is found in concentrations ranging from 0.63 to 2.9 mg/mL according to age and gender (Valentina et al., 2019; Sayuri et al., 2021; Shima et al., 2021). In response to a stimulus such as acute inflammation or oxidative stress, the basal tear flow following administration of A-B1-NPs increased dramatically because the formulation contains three times the amount of lactoferrin found in healthy tears. A-B1-NPs may give a protein concentration that lasts for a long time. This increases its bioavailability in situations where BLF content of the tears is compromised.

The presence of the P407/P188 surfactant may be responsible for minor reduction of cell viability. On the other hand, to prevent protein aggregation through production, transportation and storage, surfactants are commonly used. Polysorbates are typically regarded as GRAS, because of their well-recognized breakdown, and therefore are the most often utilized in biological products as surfactants. Based on the fact that the formulation components are typically thought to be safe, this finding backs up the biocompatibility of the produced A-B1-NPs when in contact with corneal cells.

3.6.2. *Nanoparticles' anti-inflammatory efficacy on HCE-2 cells*

NPs' capacity to reduce a reaction of inflammation caused by LPS in HCE-2 cells, was tested by measuring IL-8 and TNF-α secreted cytokines and the results are shown in Figs. 12 and 13**.** LPS generated substantial cytokine release when NPs were not present (positive control), with AMP-BLF-NPs remarkably reducing the production of both cytokines to grades comparable to those induced by AMP-BLF solution ($P < 0.05$). These findings suggested that the AMP-BLF-triblock polymers NPs had a profound anti-inflammatory impact.

There is a proof that tears contain decreased quantities of certain proteins, such as lysozyme, in many eye illnesses involving chronic inflammation or fungal infection (Roberto et al., 2019; Tamhane et al., 2019). These diseases entail the overexpression of many inflammatory markers, particularly TNF-α and IL-8 cytokines. It has been shown that increased IL-8 levels in tears drive neutrophils, basophils and T cells to migrate, provoking exacerbated symptoms (Tamhane et al., 2019). Notably, TNF-α, which is believed to be a marker of the ocular surface's overall inflammatory condition in people with various ophthalmopathy, was reported by multiple studies to be secreted in greater degrees. BLF has been demonstrated to control the expression of a variety of cytokines in a variety of ways (Ghasemi, 2018). It's been discovered that this protein interacts with inflammatory cell surface receptors. For example, BLF interacts with bacterial LPS for CD14 receptor binding, lowering NF-kB-induced transcription of multiple inflammatory mediator genes. Meanwhile, in iron sequestration, BLF and AMP can govern neutrophil and macrophage oxidative bursts which trigger the inflammatory response (Lee et al., 2020.

Chizu et al., 2019). Accordingly, combined administration of both agents has the potential to exert a synergistic anti-inflammatory effect.

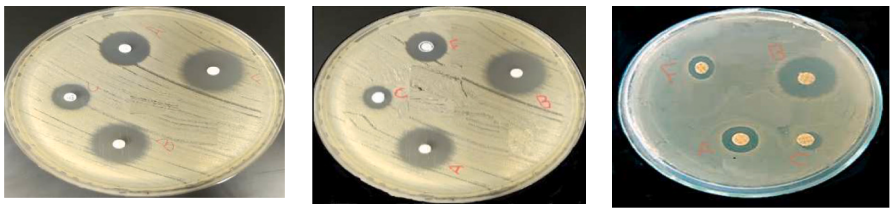

Fig. 9. *In-vitro* anti-fungal activity study for AMP in A1-NPs thermosensitive gel (A), AMP in A-B1-NPs thermosensitive gel (B), and A-B1 soluution (F) as compared to ketoconazole (C) using agar disc diffusion method.

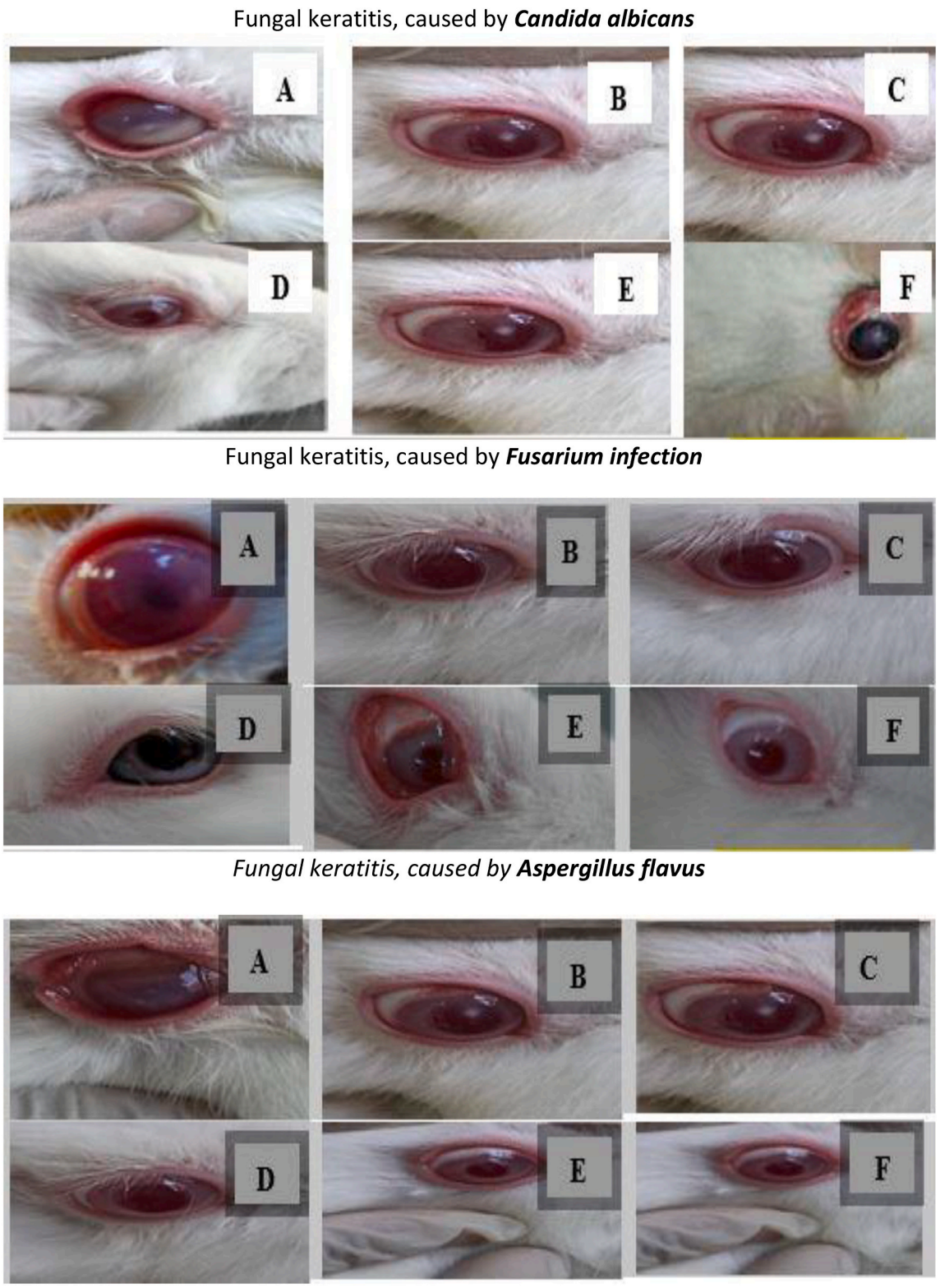

Fig. 10. A: Rabbit's cornea affected by fungal keratitis, caused by *Candida albicans, Fusarium infection, and Aspergillus flavus infection*, showing infiltration and hypopyon; B-F: Rabbit's cornea following treatment with A1-NPs thermosensitive gel, B1-NPs thermosensitive gel, A-B1-NPs thermosensitive gel, A-B1 solution and ketoconazole, showing Infiltration, and hypopyon improvement.

3.7. Histopathological study

The histological changes found in the excised corneal tissues are graphically represented in Figs. 14 (a-d) and 15 (a and b), which show the right eyes of the rabbits after receiving different treatments. The five treatment groups were differentiated based on inflammation levels: mild, moderate, and severe inflammation. Groups of rabbits that received (A1-NPs, B1-NPs, and A-B1-NPS) showed the best response against fungal colonies. In contrast, the group that received A-B1-solution and Ketoconazole performed worst. Collectively, the formula (A-B1-

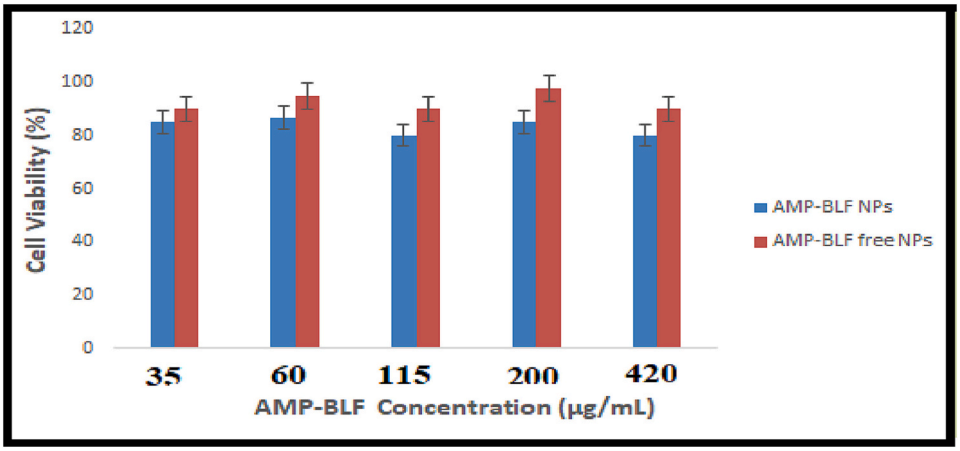

Fig. 11. Effect of thermosensitive gel containing A-B1-NPs on HCE-2 cell viability. Cell viability of 100% corresponds with untreated cell MTT average reduction value.

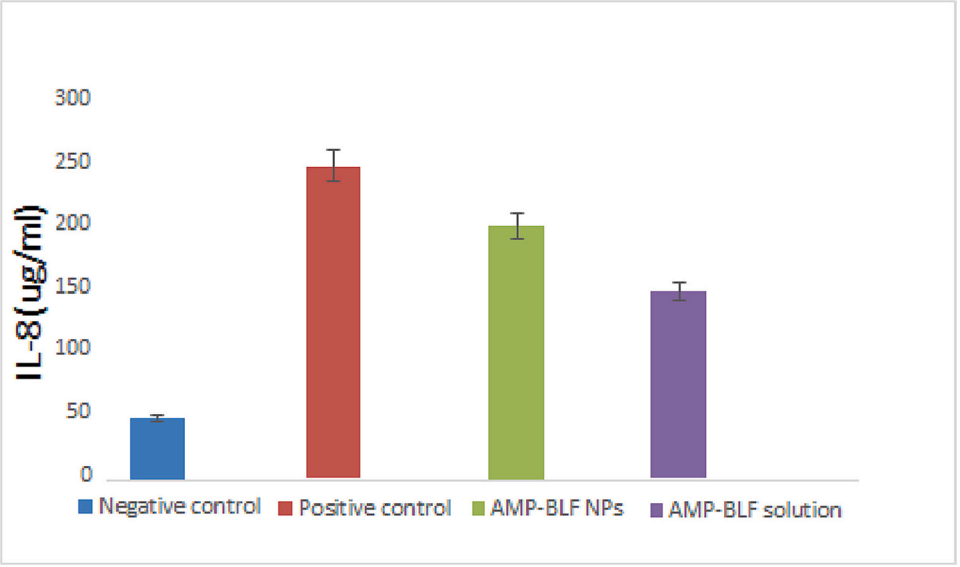

Fig. 12. Concentration of IL-8 pro-inflammatory cytokine secreted in untreated HCE-2 cells (negative control), LPS-stimulated cells (positive control), and stimulated cells treated with the thermosensitive gel containing AMP-BLF-NPs and AMP-BLF solution, respectively.

NPS) was the most effective formula during rabbit treatment against fungal colonies. Those findings were consistent with pathological studies on specimens collected from infected corneas; A-B1-NPs delivered the best results in terms of inflammation and fungal colonies. These findings suggest the efficacy of A-B1-NPs in the treatment of fungal keratitis caused by *Candida albicans, Fusarium, and Aspergillus flavus*. Adding lactoferrin as an anti-dry eye and anti-inflammatory agent relieved the inflammation associated with fungal keratitis and was more effective than the present drug preparation alone.

The results showed that A-B1-NPs have a higher cure percentage against histopathological inflammation than other formulations. This makes this formulation a suitable *candidate* for a future clinical case study with fungal keratitis to determine mucormycotic in patients with Covid −19. This combination contains AMP, which has a strong anti-fungal activity, and lactoferrin, an agent with antiviral, anti-fungal, and immune-modulatory properties. AMP-BLF is a promising *candidate* to be developed as an anti-fungal adjuvant with the potential for chemical and structural enhancements in the future.

4. Conclusions

The developed nanotechnology of Amphotericin-B and lactoferrin-loaded triblock polymers PLGA-PEG-PEI- nanoparticles combination in thermosensitive gel gives synergistic effect for treatment of fungal eye infection, conjunctivitis, and ocular Inflammation. This delivery system has proven stable with no evidence of precipitation or flocculation. In addition, the system enhances permeability across the cornea and maintains long-term release of bioactive molecules, thus improving the *in-vitro* and *in-vivo* pharmacokinetic and pharmacodynamic profile. Therefore, this combination has strong anti-fungal and immunity boosting activity so that further studies in immunocompromised patients with black fungus mucormycotic and Covid-19 are warranted.

Funding

This work was funded by the Deanship of Scientific Research at Jouf University under grant No (DSR-2021-01-03120).

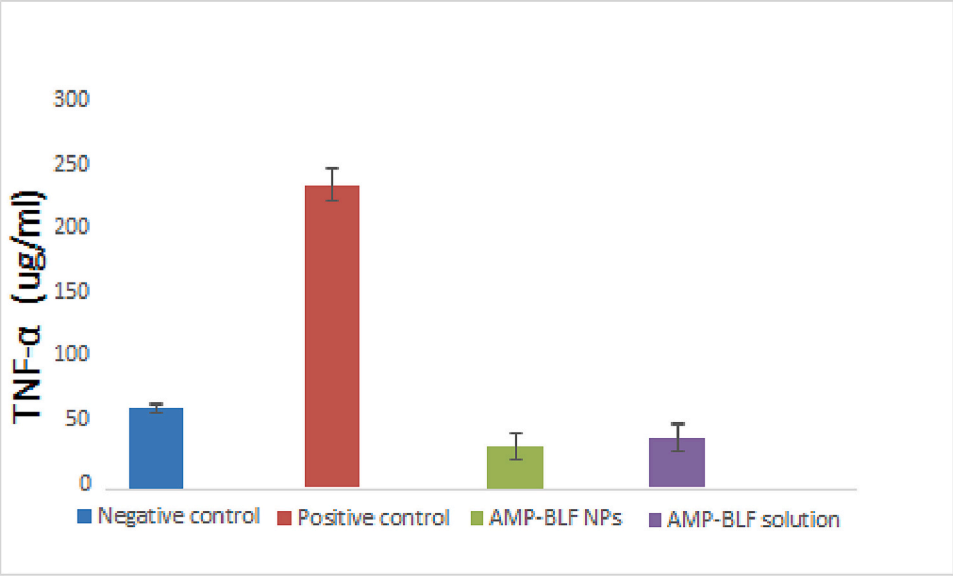

Fig. 13. Concentration of TNF-α pro-inflammatory cytokine secreted in untreated HCE-2 cells (negative control), LPS-stimulated cells (positive control), stimulated cells treated with the thermosensitive gel containing AMP-BLF-NPs and AMP-BLF solution, respectively.

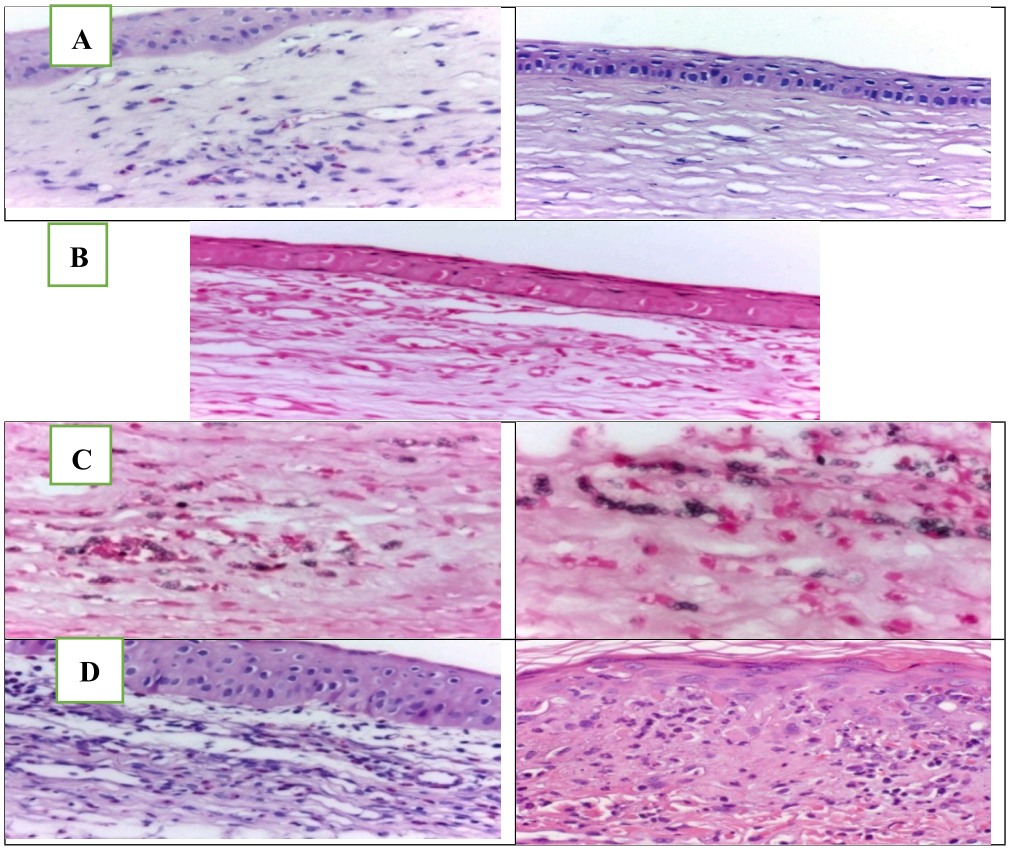

Fig. 14. A. Normal corneal stroma intact without fungal keratitis (H&E), **B**. Corneal stroma showing mild inflammatory reaction with few neutrophils from a specimen of *Candida albicans* after treatment with A1-NPs thermosensitive gel and B1-NPs thermosensitive gel (H&E), **C**. Corneal stroma negative for fungal spores of *Candida albicans* and no inflammation from a specimen after treatment with the A-B1-NPs thermosensitive gel and **D**. Corneal stroma with a moderate number of fungal spores of *Candida albicans* and moderate Inflammation after treatment with Ketoconazole and AMP-BLF-solution.

Institutional review board statement

The animal study protocol was approved by the animal care and use committee of the Faculty of Pharmacy, Cairo University, Cairo, Egypt (no. PI 2102, 2021).

Informed consent statement

Not applicable.

CRediT authorship contribution statement

Sammar Fathy Elhabal: Conceptualization, Methodology, Formal analysis, Investigation, Writing – original draft, Writing – review &

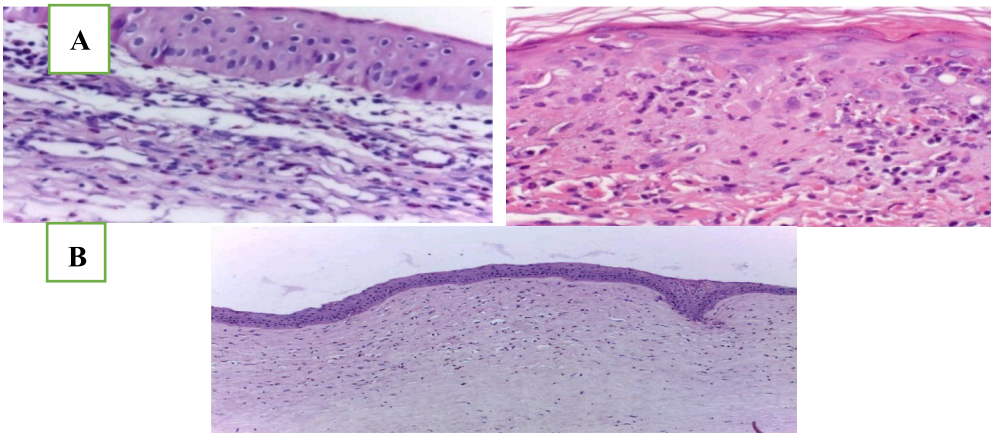

Fig. 15. A. Corneal stroma showing mild inflammatory response with mild exudation of neutrophils from a specimen of *Aspergillus flavus* after treatment with A1-NPs thermosensitive gel and B1-NPs thermosensitive gel, **B**. Corneal stroma with moderate inflammatory reaction and no fungal spores from a specimen of *Aspergillus flavus* after treatment with Ketoconazole.

editing. **Shrouk A. Ghaffar:** Conceptualization, Methodology, Formal analysis, Investigation, Writing – original draft. **Raghda Hager:** Conceptualization, Formal analysis, Writing – review & editing, Supervision. **Nahla A. Elzohairy:** Methodology, Software, Resources, Writing – review & editing, Project administration. **Mohamed Mansour Khalifa:** Methodology, Validation, Resources, Writing – review & editing, Project administration. **Passant M. Mohie:** Conceptualization, Methodology, Formal analysis, Investigation, Writing – original draft, Writing – review & editing. **Rania A. Gad:** Conceptualization, Methodology, Formal analysis, Investigation, Writing – original draft, Writing – review & editing. **Nasreen N. Omar:** Methodology, Software, Resources, Writing – review & editing, Project administration. **Mohammed H. Elkomy:** Conceptualization, Methodology, Resources, Writing – review & editing, Supervision, Project administration, Funding acquisition. **Mohammad Ahmad Khasawneh:** Methodology, Software, Resources, Writing – review & editing, Project administration. **Nashwa Abdelaal:** Methodology, Software, Resources, Writing – review & editing, Project administration.

Declaration of Competing Interest

The authors wish to declare no interest is involved in this publication.

Data availability

Data is contained within the article and supplementary materials.

Appendix A. Supplementary data

Supplementary data to this article can be found online at https://doi.org/10.1016/j.ijpx.2023.100174.

References

Ahmed, T.A., Alzahrani, M.M., Sirwi, A., Alhakamy, N.A., 2021. The antifungal and ocular permeation of ketoconazole from ophthalmic formulations containing transethosomes nanoparticles. Pharmaceutics 13 (2), 151, 6, 24.
Alaaeldin, A.H., Mohammad, K., Hanan, M.E., et al., 2022. Salvadora persica attenuates DMBA-induced mammary cancer through the downregulation of oxidative stress, estrogen receptor expression and proliferation, and augmenting apoptosis. Biomed. Pharmacother. 3, 147–112666.
Ana, L.M., Natalia, D., Amanda, C., Marta, E., Josefa, B., et al., 2021. Development of lactoferrin-loaded liposomes for the management of dry eye disease and ocular inflammation. Pharmaceutics 13 (10), 1698, 15.
Andr'es-Guerrero, V., Bravo-Osuna, I., Pastoriza, P., et al., 2017. Novel technologies for the delivery of ocular therapeutics in glaucoma. J. Drug Deliv. Sci. Technol. 42, 181–192.
Avinash, G., Kartik, T.N., Amit, A., et al., 2018. Boosted memory and improved brain bioavailability of rivastigmine: targeting effort to the brain using covalently tethered lower generation PAMAM dendrimers with lactoferrin. Mol. Pharm. 15, 4538–4549.
Bancroft, J.D.S., Turner, D.R., 2013. Theory and Practice of Histological Techniques, 7th ed. London, UK, Churchill Livingstone Elsevier.
Berthomieu, C., Hienerwadel, R., 2009. Fourier transform infrared (FTIR) spectroscopy. Photosynth. Res. 101, 157–170.
Calliandra, Md, Fernanda, G., Daniel, Z., et al., 2018. Broth microdilution in vitro screening: an easy and fast method to detect new antifungal compounds. J. Vis. Exp. 14 (132), 57127.
Cano, A., Ettcheto, M., Espina, M., et al., 2018. Epigallocatechin-3-gallate loaded PEGylated-PLGA nanoparticles: a new anti-seizure strategy for temporal lobe epilepsy. Nanomedicine 14, 1073–1085.
Cano, A., Ettcheto, M., Chang, J.H., et al., 2019. Dual-drug loaded nanoparticles of Epigallocatechin-3-gallate (EGCG)/Ascorbic acid enhance therapeutic efficacy of EGCG in a APPswe/PS1dE9 Alzheimer's disease mice model. J. Control. Release 301, 62–75.
Carvajal-Vidal, P., F'abrega, M.J., Espina, M., et al., 2019. Development of Halobetasol-loaded nanostructured lipid carrier for dermal administration: Optimization, physicochemical and biopharmaceutical behavior, and therapeutic efficacy. Nanomedicine 20, 1–10.
Chen, X., Aqrawi, L.A., Utheim, T.P., Tashbayev, B., Utheim, Ø.A., Reppe, S., Hove, L.H., Herlofson, B.B., Singh, P.B., Palm, Ø., et al., 2019. Elevated cytokine levels in tears and saliva of patients with primary Sjögren's syndrome correlate with clinical ocular and oral manifestations. Sci. Rep. 9, 7319.
Chizu, F., Hiroto, M., Yasushi, O., et al., 2019. Liposomal amphotericin b fosters the corticosteroids' anti-inflammatory effect on murine allergic bronchopulmonary aspergillosis model airways. Inflammation 42, 2065–2071.
Christopher, D., Eduardo, A., Ramesh, S.A., et al., 2021. Fungal keratitis: mechanisms of infection and management strategies. Surv. Ophthalmol. 20:S0039–6257 (21), 00175–2.
David, J.E., Jeffrey, J.S., Thomas, R.V., et al., 2019. Analytical method for lactoferrin in milk-based infant formulas by signature peptide quantification with ultra-high-performance LC-tandem mass spectrometry. J. AOAC Int. 02, 915–925.
Desiree, V.H., Wenlei, J., Thilak, M., 2019. Evaluation of size-based distribution of drug and excipient in amphotericin B liposomal formulation. Int. J. Pharm. 5, 569–118603.
Diaz-Garrido, N., Fabrega, M.J., Vera, R., Giménez, R., Badia, J., Baldomà, L., et al., 2019. Membrane vesicles from the probiotic Nissle 1917 and gut resident Escherichia coli strain distinctly modulate human dendritic cells and subsequent T cell responses. J. Funct. Foods 61, 1–12.
El-Desouky, M., Osman, S., Shams Eldin, N.M., Emaraa, I., 2017. Arginase enzyme activity and lactoferrin protein concentration in egyptian diabetic patients. Int. J. Adv. Res. 5, 1518–1523.
Elsayed, I., Sayed, S., 2017. Tailored nanostructured platforms for boosting transcorneal permeation: box-Behnken statistical optimization, comprehensive in vitro, ex vivo, and in vivo characterization. Int. J. Nanomedicine 12, 7947–7962.
Emily, C., Nicola, L., Declan, F., et al., 2020. Severe corneal melting after cataract surgery in patients prescribed topical postoperative NSAIDs and dexamethasone/neomycin combination therapy. J Cataract Refract Surg 46, 138–142.
Falah, H., Obayes, A.K., 2020. Amphotericin B as antiviral drug: possible efficacy against COVID-19. Ann. Thorac. Med. 15, 118–124.
Fu, Y., Kao, W.J., 2010. Drug release kinetics and transport mechanisms of non-degradable and degradable polymeric delivery systems. Exp. Opin. Drug Deliv. 7, 429–444.
Ghadi, R., Dand, N., 2017. (2017) BCS class IV drugs: Highly notorious candidates for formulation development. J. Control. Release 248, 71–95.
Ghasemi, H., 2018. Roles of IL-6 in ocular inflammation: a review. Ocul. Immunol. Inflamm. 26, 37–20.

Ghobad, M., Mostafa, F., Pardis, M., et al., 2021. Preparation, physicochemical characterization and anti-fungal evaluation of amphotericin B-loaded PLGA-PEG-galactosamine nanoparticles. Adv. Pharm. Bull. 11, 311–317.
G'omez-Segura, L., Parra, A., Calpena-Campmany, A.C., et al., 2020. Ex vivo permeation of carprofen vehiculated by PLGA nanoparticles through porcine mucous membranes and ophthalmic tissues. Nanomaterials 10, 16.
Gonzalez-Pizarro, R., Silva-Abreu, M., Calpena, A.C., et al., 2018. Development of fluorometholone-loaded PLGA nanoparticles for treatment of inflammatory disorders of anterior and posterior segments of the eye. Int. J. Pharm. 547, 338–346.
Gonzalez-Pizarro, R., Carvajal-Vidal, P., Halbault, L., et al., 2019a. In-situ forming gels containing fluorometholone-loaded polymeric nanoparticles for ocular inflammatory conditions. Colloids Surf. B: Biointerfaces 175, 365–374.
Gonzalez-Pizarro, R., Parrotta, G., Vera, R., et al., 2019b. Ocular penetration of fluorometholone-loaded PEG-PLGA nanoparticles functionalized with cell-penetrating peptides. Nanomedicine 14, 3089–3104.
Janagam, D.R., Wu, L., Lowe, T.L., 2017. Nanoparticles for drug delivery to the anterior segment of the eye. Adv. Drug Deliv. Rev. 122, 31–64.
Julia, A.K., George, E.H., Max, S., et al., 2000. Use of the national committee for clinical laboratory standards guidelines for disk diffusion susceptibility testing in New York State laboratories. J. Clin. Microbiol. 38, 3341–3348.
Katrien, V.D., Patrick, V.D., Greetje, V.V., 2020. Bioluminescence imaging to study mature biofilm formation by Candida Spp. and antifungal activity in vitro and in vivo. Methods Mol. Biol. 2081, 127–143.
Kenya, E.F., Richard, J.P., Dee, A.C., 2020. Lactoferrin-derived peptide lactofungin is potently synergistic with amphotericin. Antimicrob. Agents Chemother. 21 (64), 00842–20.
Lamprecht, A., Ubrich, N., Hombreiro P'erez, M., et al., 2000. Influences of process parameters on nanoparticle preparation performed by a double emulsion ultrasonication technique. Int. J. Pharm. 196, 177–182.
Lee, J., Lee, J., Lee, S., et al., 2020. Bioactive membrane immobilized with lactoferrin for modulation of bone regeneration and inflammation. Tissue Eng. - Part A 26, 1243–125.
Lemp, M.A., Foulks, G.N., 2007. The definition and classification of dry eye disease: Report of the Definition and classification Subcommittee of the International Dry Eye WorkShop. Ocul. Surf 5, 75–92.
Malatesta, M., 2016. Transmission electron microscopy for nanomedicine: Novel applications for long-established techniques. Eur. J. Histochem. 9, 2751.
Marcelle, S., Ana, C.C., Marta, E., et al., 2018. Optimization, biopharmaceutical profile and therapeutic efficacy of pioglitazone-loaded PLGA-PEG nanospheres as a novel strategy for ocular inflammatory disorders. Pharm. Res. 35 (1), 11.
Masoudipour, E., Kashanian, S., Hemati, A., et al., 2017. Surfactant effects on the particle size, zeta potential, and stability of starch nanoparticles and their use in a pH-responsive manner. Cellulose 24, 4217–4234.
Mohamed, M., Abdullah, H., Aliyah, A., Yousef, A., Amal, E., 2022. Novel metoprolol-loaded chitosan-coated deformable liposomes in thermosensitive in situ gels for the management of glaucoma: a repurposing approach. Gel. 7;8 (10), 635.
Montenegro, L., Castelli, F., Sarpietro, M.G., 2018. Differential scanning calorimetry analyses of idebenone-loaded solid lipid nanoparticles interactions with a model of bio-membrane: a comparison with in vitro skin permeation data. Pharmaceuticals 11, 138.
Mrittika, S., Santosh, G.H., Namrata, S., Mahipal, S.S., 2021. COVID-19 and eye: a review of ophthalmic manifestations of COVID-19. Indian J. Ophthalmol. 69, 488–509.
Raghavendra, C.M., Ramesh, B., Vidhya, R., et al., 2008. Nano/micro technologies for delivering macromolecular therapeutics using poly(D, L-lactide-co-glycolide) and its derivatives. J. Control. Release 125, 193–209.
Rajendra, P., Abdul, H.S., Manpreet, K.R., 2016. Antifungals: mechanism of action and drug resistance. Adv. Exp. Med. Biol. 892, 327–349.
Rebecca, L.M., Rachael, W.S., 2013. PLGA nanoparticles are formed by single- or double-emulsion with vitamin E-TPGS. J. Vis. Exp. 27, 82–51015.
Rehab, A., Sammar, F.E., Nevine, S.A., et al., 2021. Formulation and characterization of acetazolamide/carvedilol niosomal gel for glaucoma treatment: in vitro, and in vivo study. Pharmaceutics 5, 13–221.
Revu, V.L.N., Pritikana, J., Neha, T., et al., 2021. Carboplatin- and etoposide-loaded lactoferrin protein nanoparticles for targeting cancer stem cells in retinoblastoma in vitro. Invest. Ophthalmol. Vis. Sci. 62, 14–13.
Roberto, G., Graziella, P., Rodrigo, V., et al., 2019. Ocular penetration of fluorometholone-loaded PEG-PLGA nanoparticles functionalized with cell-penetrating peptides. Nanomedicine (London) 14, 3089–3104.
Sammar, E., Hanan, E., Soha, H., Ahmed, E., Alaaeldin, H., Mohammad, K., 2022. Biosynthesis and characterization of gold and copper nanoparticles from salvadora persica fruit extracts and their biological properties. Drug Deliv. 6095–6112.
Sanaa, E., Mohamed, O., Sammar, I., 2018. Effect of cosolvents on the absorptive clearance of ketotifen fumarate from rabbit intestine, in-situ. J. Adv. Pharm. Res. 2, 168–179.
S'anchez-L'opez, E., Egea, M.A., Cano, A., et al., 2016. PEGylated PLGA nanospheres optimized by design of experiments for ocular administration of dexibuprofen-in vitro, ex vivo and in vivo characterization. Colloids Surf. B: Biointerfaces 145, 241–250.
Sayuri, N.B., Denisse, A.G., Elisa, R.E., et al., 2021. Recombinant human lactoferrin carrying humanized glycosylation exhibits antileukemia selective cytotoxicity, microfilament disruption, cell cycle arrest, and apoptosis activities. Investig. New Drugs 39, 400–415.
Seyfoddin, A., Al-Kassas, R., 2013. Development of solid lipid nanoparticles and nanostructured lipid carriers for improving ocular delivery of acyclovir. Drug Dev. Ind. Pharm. 39, 508–519.
Shengtao, S., Qixue, L., Lei, H., et al., 2018. Identification and characterization of fusarium proliferatum, a new species of fungi that cause fungal keratitis. Sci. Rep. 20, 8–4859.
Shima, A.K., Samira, S., Pooya, G.N.A., 2021. Comparison of antifungal and cytotoxicity activities of titanium dioxide and zinc oxide nanoparticles with amphotericin B against different Candida species: in vitro evaluation. J. Clin. Lab. Anal. 35, e23577.
Soni, V., Pandey, V., Tiwari, R., et al., 2019. Design and evaluation of ophthalmic delivery formulations. In: Basic Fundamentals of Drug Delivery. Elsevier Inc, pp. 473–538.
Swarnali, D., Suresh, Preeti K., et al., 2010. Design of Eudragit RL 100 nanoparticles by nanoprecipitation method for ocular drug delivery. Nanomedicine. 6 (2), 318–323.
Tamhane, M., CabreraGhayouri, S., Abelian, G., Viswanath, V., 2019. Review of biomarkers in ocular matrices: challenges and opportunities. Pharm. Res. 36, 1–35.
Tapia-Guerrero, Y.S., Del Prado-Audelo, M.L., Borbolla-Jim'enez, F.V., et al., 2020. Effect of UV and gamma irradiation sterilization processes in the properties of different polymeric nanoparticles for biomedical applications. Materials (Basel) 13, 1–19.
Thi, H.Y.T., Thi, T.G.V., Thi, M.H.P., 2021. Preparation and characterization of liposomes double-loaded with amphotericin B and amphotericin B/hydroxypropyl-beta-cyclodextrin Inclusion complex. Pharm. Nanotechnol. 9, 236–244.
Valentina, P., Silvia, T., Marzia, L., 2019. Lactoferrin-loaded contact lenses counteract cytotoxicity caused in vitro by keratoconic tears. Cont Lens Anterior Eye 42, 253–257.
Vega, E., Egea, M.A., Calpena, A.C., Espina, M., García, M.L., 2012. Role of hydroxypropyl- β -cyclodextrin on freeze-dried and gamma-irradiated PLGA and PLGA – PEG diblock copolymer nanospheres for ophthalmic flurbiprofen delivery. Int. J. Nanomedicine 7, 1357–1371.
Vogelsinger, H., Weiler, S., Djanani, A., Kountchev, J., Bellmann-Weiler, R., Wiedermann, C.J., Bellmann, R., 2006. Amphotericin B tissue distribution in autopsy material after treatment with liposomal amphotericin B and amphotericin B colloidal dispersion. J. Antimicrob. Chemother. 6;57 (6), 1153–1160.
Wang, B., Timilsena, Y.P., Blanch, E., Ad hikari B., 2019. Lactoferrin: Structure, function, denaturation, and digestion. Crit. Rev. Food Sci. Nutr. 59, 580–585.
Zhen, L., Zhen, Z., Jingjing, Y., et al., 2021. Assessment of the antifungal effects in vitro and the ocular pharmacokinetics of solid-lipid nanoparticle in rabbits. Int. J. Nanomedicine 16, 7847–7857.